

RNF220 is required for cerebellum development and regulates medulloblastoma progression through epigenetic modulation of Shh signaling

Pengcheng Ma^{1,7}, Tao An^{2,7}, Liang Zhu¹, Longlong Zhang^{1,3}, Huishan Wang^{1,3}, Biyu Ren^{1,4}, Bin Sun⁵, Xia Zhou⁵, Yan Li^{2,*} and Bingyu Mao^{1,6,*}

¹State Key Laboratory of Genetic Resources and Evolution, Kunming Institute of Zoology, Chinese Academy of Sciences, Kunming 650223, China

²State Key Laboratory of Phytochemistry and Plant Resources in West China, Kunming Institute of Botany, Chinese Academy of Sciences, Kunming 650201, China

³Kunming College of Life Science, University of Chinese Academy of Sciences, Kunming 650203, China

⁴Institute of Health Sciences, Anhui University, Hefei 230601, China

⁵Key Laboratory of Animal Models and Human Disease Mechanisms of the Chinese Academy of Sciences & Yunnan Province, Kunming Institute of Zoology, Kunming 650223, China

⁶Center for Excellence in Animal Evolution and Genetics, Chinese Academy of Sciences, Kunming 650223, China

⁷These authors contributed equally to this work.

* Correspondence:

Bingyu Mao: mao@mail.kiz.ac.cn

Yan Li: liyanb@mail.kib.ac.cn

ABSTRACT

Sonic hedgehog (Shh) signaling is essential for proliferation of cerebellar granule neuron progenitors (CGNPs) and its mis-regulation is linked to various disorders, including cerebellar cancer medulloblastoma (MB). We recently identified RNF220, an ubiquitin E3 ligase promoting K63-linked polyubiquitination and nuclear exportation of Glis, as a Shh/Gli regulator involved in ventral neural patterning. Here, we report that RNF220 is required for the proliferation of CGNPs and Daoy cells (a Shh-grouped MB cell line), where it works as a positive regulator of Shh signaling. Mechanistic investigation demonstrated that RNF220 promotes Shh target gene expression by targeting the PRC2 component EED and alters levels of epigenetic modification marks on Shh target promoters. We provided evidence that RNF220^{+/-}; Ptch1^{+/-} mice showed lower spontaneous MB occurrence comparing to Ptch1^{+/-} mice. Furthermore, in human clinical MB samples, RNF220 expression correlated well with that of GAB1, a Shh-group MB marker. Our findings provide new insights into the epigenetic regulation of Shh signaling and identified RNF220 as a potential new diagnostic marker and therapeutic target for Shh-group MB.

KEYWORDS: RNF220, cerebellum, Sonic hedgehog, EED, medulloblastoma

INTRODUCTION

Sonic hedgehog (Shh) signaling plays critical roles in specifying spatial patterns and cell fate determination during embryonic development and in maintaining tissue homeostasis in adults (Fuccillo et al., 2006; Hui and Angers, 2011; Ingham and Placzek, 2006; Pasca di Magliano and Hebrok, 2003; Ruiz i Altaba et al., 2002; Vaillant and Monard, 2009). A myriad of birth defects and cancer syndromes are associated with genetic lesions in genes that transduce Shh signaling (Briscoe and Therond, 2013; Fuccillo et al., 2006; Hui and Angers, 2011; Kim et al., 2018; Northcott et al., 2012; Pasca di Magliano and Hebrok, 2003; Ruiz i Altaba et al., 2002).

During normal cerebellar development, Shh acts as a mitogen and stimulates proliferation of cerebellar granule neuron precursors (CGNPs) (Ruiz et al., 2002; Vaillant and Monard, 2009; Wang and Zoghbi, 2001). CGNPs are specified starting at mouse embryonic day 13.5 (E13.5) and then undergo intense Shh-driven proliferation at the external granular layer (EGL) before becoming post-mitotic and migrating inward to form the internal granular layer (IGL) of the mature cerebellum (Vaillant and Monard, 2009). Mutations resulting in overactivation and/or deregulation of Shh signaling, including loss of patched 1 (Ptc1), alters the development of CGNPs, making them hyper-proliferative and susceptible to malignant transformation into medulloblastoma (MB), the most common malignant pediatric brain tumor (Gajjar and Robinson, 2014; Louis et al., 2016; Vaillant and Monard, 2009). The identification of four genetic subgroups of MB provided a rationale for studying molecular-based

therapies in an effort to improve disease survival and reduce treatment-related side effects (Gajjar and Robinson, 2014; Northcott et al., 2017; Northcott et al., 2012). Moreover, as over-activated Shh signaling causes about 30% of MBs (Louis et al., 2016; Northcott et al., 2012), the biological and pathogenic importance of Shh signaling emphasizes the need to tightly control its action.

Shh signaling is activated upon the binding of the Shh ligand to its receptor Ptch1, leading to the release of Smoothed (Smo) inhibition and activation of intracellular signals, including the Gli transcription factors (Hui and Angers, 2011; Pasca di Magliano and Hebrok, 2003). There are three Glis (Gli1–3) in mammals; Gli2 and Gli3 are bifunctional and function as transcriptional activators (GliA) in their full length forms and as repressors (GliR) in their truncated forms. Gli1 lacks the N-terminal repressor domain and functions exclusively as an activator (Hui and Angers, 2011). Shh signaling is regulated at multiple levels, ranging from the Shh ligand to the downstream Gli transcription factors. In addition, epigenetic regulation plays important roles in Shh target genes activation. In the absence of Shh signaling, Gli target genes are marked by repressive histone marks by the polycomb repressive complex 2 (PRC2) (Shi et al., 2014). The PRC2 complex contains three essential subunits, the SET-domain-containing protein EZH1/2, the Zinc-finger protein SUZ12, and the WD40 protein EED (Lanzuolo and Orlando, 2012). Knockdown of SUZ12 or knockout of EZH2 increases the expression of Shh target genes, whereas increasing the local PRC2 concentration represses Shh target gene expression (Shi et al., 2014). Upon

Shh activation, lysine demethylase 6 B (KDM6B) is recruited to the promoter regions by Gli proteins, where it replaces PRC2 and removes repressive histone marks, thereby activating gene transcription (Shi et al., 2014). In addition, Gli1 also recruits lysine acetyltransferase 2 B (KAT2B), which increases active AcH3K9 marks in response to Shh/Gli signaling. Both KDM6B and KAT2B are required for the activation of Shh target genes and MB progression (Malatesta et al., 2013; Shi et al., 2014).

We previously identified RNF220, an ubiquitin E3 ligase involved in ventral neural patterning, as a new Gli regulator that promotes K63-linked polyubiquitination and nuclear exportation of Gli (Ma et al., 2019b). Recently, we reported that RNF220/ZC4H2 complex is required for central noradrenergic neuron development by targeting Phox2a/2b for monoubiquitination (Song et al., 2020). Here, we studied the roles of RNF220 in Shh signaling during cerebellum development and medulloblastoma progression. Unexpectedly, we found that RNF220 promotes Shh target gene expression epigenetically in these processes through targeting EED for degradation, overwriting its effects on Gli ubiquitination. We provided evidence that RNF220 might be involved in MB development in a mouse model as well as clinical samples.

RESULTS

RNF220 is required for CGNP proliferation and cerebellum development

We first examined the expression of RNF220 during mouse cerebellum development and found that RNF220 was specifically expressed in the proliferating CGNPs at the external granular layer (EGL) of the developing cerebellum (Fig. 1A and 1B). In RNF220^{-/-} mouse embryos at P0 stage, the cerebellum shows a defective foliation and the perimeter of the cerebellum was reduced (Fig. 1C and 1D) (Quaranta et al., 2017), suggesting that RNF220 may be involved in CGNP proliferation. We isolated the CGNPs of the P7 cerebellum from Rosa26-CreER and RNF220^{fl/fl}; Rosa26-CreER mice and examined the effect of RNF220 deletion induced by 4-OHT treatment on CGNP proliferation. We found that 4-OHT treatment for 3 days efficiently decreased RNF220 expression in RNF220^{fl/fl}; Rosa26-CreER CGNPs (Fig. S1A and S1B). We also found that 4-OHT treatment significantly decreased the BrdU incorporation ratio of RNF220^{fl/fl}; Rosa26-CreER CGNPs but had no effect on Rosa26-CreER CGNPs (Fig. S1C and S1D). To confirm these results, we carried out staining assays with Ki-67, a marker for proliferating cells, and obtained the same results (Fig. S1E and S1F). As CGNP proliferation is mainly driven by Shh signaling during cerebellum development (Hui and Angers, 2011; Vaillant and Monard, 2009), we next examined Shh signal levels in RNF220-knockout CGNPs. RNF220 knockout reduced the expression levels of Gli1, Ptch1 and Hhip1, three established Shh signaling targets (Fig. S1G-S1I). Next, we carried out BrdU pulse labeling assays in P0

cerebellum and found that both the BrdU positive cell number and BrdU incorporation ratio decreased in RNF220^{-/-} cerebellums compared to controls (Fig. 1E-1G). Also, realtime PCR assays shows that the expression levels of Gli1, Ptch1 and Hhip1 in P0 cerebellums decreased in RNF220^{-/-} pups compared to controls (Fig. 1H-1J). These results indicate that RNF220 is required for cerebellum development by modulating Shh signaling in CGNPs.

RNF220 contributes to Shh-group MB progression

Aberrant or sustained Shh signaling in CGNPs usually results in MB occurrence; thus, we tested the effect of RNF220 on the progression of Shh-group MB. We performed Dox-induced shRNA mediated RNF220 knockdown experiments in Daoy cells, a MB cell line classified as Shh subtype (Ivanov et al., 2016). The shRNA knockdown efficiency on RNF220 mRNA and protein levels was demonstrated by RT-PCR and Western blotting (Fig. S2A and S2B). Cell proliferation was inhibited by RNF220 knockdown, as evidenced by the growth curve (Fig. 2A) and BrdU incorporation analysis (Fig. 2B and 2C). In addition, Dox-induced RNF220 knockdown significantly attenuated colony formation capacity (Fig. 2D and 2E) and reduced Gli1, Ptch1 and Hhip1 levels in Daoy cells (Fig. 2F-2H). To test the role of RNF220 in MB progression, we injected Daoy cells stably transfected with inducible RNF220 shRNA into mice and induced RNF220 knockdown with Dox. Dox treatment led to inhibited tumor growth and decreased tumor size *in vivo* (Fig. 2I and 2J). Note that Dox treatment did not affect mouse growth, as evidenced by their body weight (Fig.

S2C). RNF220 knockdown was efficiently induced in the tumors as RNF220 protein expression was found decreased (Fig. S2D).

To further explore the involvement of RNF220 in MB genesis, we utilized a spontaneous orthotopic MB model driven by aberrant Shh signaling in *Ptch1*^{+/-} mice (Lisa et al., 1997). *Ptch1* expression was significantly reduced in the MB tissue compared with normal cerebellum tissue (Fig. S2E). Highly activated Shh signaling was evidenced by the increased mRNA levels of *Gli1* and *Hhip1*, two established Shh signaling targets (Fig. S2F and S2G). Although RNF220 mRNA levels were decreased in *Ptch1*^{+/-} MB tissues (Fig. S2H), the RNF220 protein was markedly up-regulated (Fig. 5C), which suggests that RNF220 is stabilized at a post-translational level in MBs. We examined the medulloblastoma occurrence of *Ptch1*^{+/-} and *RNF220*^{+/-}; *Ptch1*^{+/-} mice during the first 12 months after birth. *RNF220*^{+/-}; *Ptch1*^{+/-} mice are less prone to medulloblastoma than *Ptch1*^{+/-} mice while the tested *RNF220*^{+/-} mice showed absolutely no medulloblastoma occurrence for the whole year (Fig. 3A). We compared the expression levels of *Gli1*, *Ptch1* and *Hhip1* using realtime PCR assays and the results showed that all the three genes were down-regulated in the *RNF220*^{+/-}; *Ptch1*^{+/-} medulloblastomas compared to those of *Ptch1*^{+/-} (Fig. 3B-3D). We then examined whether high RNF220 expression is associated with human clinical MBs. Shh-group MBs are identified by GAB1 staining (Zhang et al., 2018). Immunohistochemical staining showed a positive correlation between RNF220 and

GAB1 in clinical MBs (Fig. 3E and 3F), suggesting an involvement of high RNF220 expression in the pathogenesis of Shh-group MBs.

RNF220 positively regulates Shh signaling epigenetically

Our previous work demonstrated that RNF220 targets Glis for K63-linked polyubiquitination and promotes Glis nuclear exportation and indicated that RNF220 is involved in ventral spinal cord patterning (Ma et al., 2019b). Here, we examined whether the RNF220-mediated Gli polyubiquitination held true in CGNPs and Daoy cells. RNF220 knockout in CGNPs reduced K63-linked polyubiquitinated Glis (including both GliA and GliR) levels and increased Glis levels in nuclear fractions but did not affect total Glis levels (Fig. S3A–C). In Daoy cells, knockdown of RNF220 also decreased Glis ubiquitination and increased nuclear Glis levels (Fig. S3D–F). In contrast to increased nuclear Glis, however, knockout or knockdown of RNF220 decreased Gli target gene expression in both CGNPs and Daoy cells (Fig. S1G-S1I and 2F-2H), which is in contrast to what was observed in neural stem cells (Ma et al., 2019b). Therefore, it is possible that other RNF220-mediated mechanisms downstream of Glis exist wherein RNF220 is a positive regulator of Shh signaling in CGNPs and Daoy cells.

Shh signaling induces an epigenetic switch from transcriptional repression to activation that is required for Gli to activate target gene expression (Shi et al., 2014). We thus examined whether RNF220 may affect the epigenetic status of Shh target gene promoters by employing ChIP-PCR in both CGNP and Daoy cells (Fig. 4 and S4). The

results showed that 4-OHT mediated RNF220 knockout in CGNPs or shRNA-mediated RNF220 knockdown in Daoy cells reduced permissive marks, such as H3K4me3, AcH3K27, and AcH3K4, and increased repressive marks, such as H3K27me3 and H3K9me3, at the *Gli1*, *Ptch1* and *Hhip1* promoter regions (Fig. 4 and S4). Consistent with a previous report, activating the Shh pathway by SAG increased *Gli1* binding to the promoter of Shh signaling targets in both CGNPs and Daoy cells (Fig. 4 and S4). These results suggest that RNF220 may epigenetically facilitate *Gli* target gene expression, bypassing its effect on *Gli* ubiquitination and nuclear export to limit *Gli* activity in CGNPs and Daoy cells.

RNF220 targets EED for polyubiquitination and proteasomal degradation

The PRC2 complex is involved in the epigenetic control of Shh target gene regulation (Shi et al., 2014). We thus examined the protein levels of PRC2 complex proteins in CGNPs or Daoy cells after RNF220 knockout by 4-OHT treatment or knockdown by shRNA, respectively. EED protein levels were found up-regulated while EZH2 and SUZ12 protein levels remained the same as in control cells (Fig. 5A and 5B). Similar results were obtained when the *Ptch1*^{+/-} MB and control cerebellum tissues were compared (Fig. 5C). Moreover, co-immunoprecipitation (co-IP) assays indicated that RNF220 interacts with EED both *in vitro* and *in vivo* in CGNPs, Daoy, HEK293 cells and E18.5 mouse cerebellum tissues (Fig. 5D-5G and S5A-S5B). We further carried out *in vivo* ubiquitination assays to test whether RNF220 targets EED for polyubiquitination. Overexpression of RNF220 wild-type, but not the ligase-dead

mutant, promotes EED polyubiquitination modification in HEK293 cells (Fig. 5H). Ubiquitin ligases can add different types of ubiquitin chains to their substrates, and K48-linked polyubiquitination chains target proteins for degradation. As shown in Fig. 5H, RNF220 efficiently promoted EED ubiquitination only when the lysine at position 48 (K48) remained in the ubiquitin molecule but not when K48 was mutated (K48R), suggesting that RNF220 targets EED for K48-linked polyubiquitination (Fig. 5H). To confirm endogenous RNF220-mediated ubiquitination of EED, we analyzed the ubiquitination of endogenous EED in control and RNF220 knockout/knockdown CGNP or Daoy cells. As expected, the ubiquitination of endogenous EED was reduced in RNF220 knockout CGNP, RNF220 knockdown HEK293 and Daoy cells compared with that in control cells (Fig. 5I, 5J and S5C). Also, the ubiquitination level of endogenous EED in *Ptch1*^{+/-} medulloblastoma tissues increased compare to that of control cerebellum tissues (Fig. S5D). Collectively, these results suggest that RNF220 may epigenetically facilitate Gli target gene expression by targeting EED during cerebellum development and MB progression.

EED knockdown rescues RNF220 knockdown induced Shh signaling repression

To confirm Shh signaling repression by RNF220 knockdown is dependent on its modulation on EED in CGNPs and Daoy cells, we carried out rescue experiments by knockdown RNF220 and EED simultaneously. Firstly, we examined the siRNA-mediated knockdown efficiency by realtime RT-PCR and found that the relative expression of both RNF220 and EED significantly reduced by siRNA

transfection in both CGNPs (Fig. 6A and 6B) and Daoy cells (Fig. S6A and S6B). Interestingly, realtime RT-PCR results showed that EED knockdown rescued the Gli1, Ptch1 and Hhip1 repression mediated by RNF220 knockdown in both CGNPs (Fig. 6C-E) and Daoy cells (Fig. S6C-S6E). In addition, the epigenetic modification changes on Gli1, Ptch1 and Hhip1 promoters were rescued by EED knockdown in RNF220 knockdown CGNPs (Fig. 6F-6H) and Daoy cells (Fig. S6F-S6H). Therefore, the changes of epigenetic modification marks mediated by RNF220 knockout in CGNPs or RNF220 knockdown in Daoy cells might be due to the enhanced EED protein accumulation.

EED knockdown down-regulates Shh signaling epigenetically

At last, we examined the effect of EED knockdown on Shh signaling transduction in both CGNPs (Fig. 7) and Daoy cells (Fig. S7). Realtime PCR assays showed that the Shh signaling target genes Gli1, Ptch1 and Hhip1 was up-regulated by EED knockdown in both cells (Fig. 7A-7D and Fig. S7A-S7D). Also, the epigenetic modification changed accordingly when endogenous EED was knocked down, i.e. the active markers (H3K4me3, AcH3K4 and AcH3K27) accumulated while the repressive markers (H3K9me3 and H3K27me3) decreased (Fig. 7E-7G and Fig. S7E-S7G), implying the repressive role of EED on Shh signaling in CGNPs and Daoy cells.

DISCUSSION

In this study, we reported the involvement of RNF220 in cerebellum development and Shh-group MB progression through epigenetic regulation of Shh target gene expression by targeting the PRC2 member EED. Our work suggests RNF220 as a new potential drug target for Shh-group MB treatment.

Shh signaling is a tightly regulated process in CGNPs wherein proliferative signals are activated during the early phase of growth and deactivated when no longer necessary, ensuring cell homeostasis during cerebellum development (Vaillant and Monard, 2009). The co-expression of RNF220 with Ki-67 in the EGL is indicative of a positive role played by RNF220 in proliferative regions of the cerebellum. Indeed, we validated the proliferation-promoting role of RNF220 in *in vitro* cultured CGNPs by BrdU incorporation and Ki-67 staining assays. We attributed this activity of RNF220 to its enhancement of Shh signaling as RNF220 knockout reduced the expression of Shh target genes.

The role of RNF220 in cell proliferation and Shh signaling regulation was then confirmed by knockdown experiments in Daoy cells, an Shh-group MB cell line. In human clinical MBs, the expression level of RNF220 positively correlated with that of GAB1, a marker for Shh-group MB, supporting the involvement of RNF220 in the pathogenesis of Shh-group MB. Furthermore, we found that RNF220 protein levels increased in MB tissues from *Ptch1*^{+/-} mice, likely due to a post-translational regulation mechanism as the RNF220 mRNA levels decreased in these tissues.

Our previous work has demonstrated that RNF220 targets Glis for K63-linked polyubiquitination and thus enhances their nuclear exportation (Ma et al., 2019b). Although this mechanism holds true in both CGNPs and Daoy cells (Fig. S3), RNF220 robustly acts as a positive regulator for Shh signaling. A local epigenetic switch from PRC2 to Jmjd3 at target gene promoters induced by Shh signaling is critical for the activation of Shh target gene expression (Shi et al., 2014). In Daoy cells or CGNPs, RNF220 knockdown or knockout leads to accumulation of more repressive and less activating histone modifications at the target gene promoter regions. We showed evidence that this effect of RNF220 is likely mediated by EED, a PRC2 subunit, which was found to be an RNF220 target for polyubiquitination and degradation. Thus, in addition to promoting Gli ubiquitination and nuclear exportation to limit Gli signaling, RNF220 may also facilitate Gli target gene expression epigenetically *via* EED. The actual effect of RNF220 on Shh signaling may depend on the balance between the two mechanisms involved in a complex scenario. Different from the case of Daoy cells and CGNPs, knockout of RNF220 in neural stem cells leads to stimulation of Gli target genes (Ma et al., 2019b). Consistent with this observation, we found that the epigenetic markers at the Gli target promoters were not affected by RNF220 knockout in neural stem cells, neither were the expression levels of EED (Fig. S8 and S9). Intriguingly, we did not detect interaction between RNF220 and EED in neural stem cells (Fig. S8). And although SAG alone did promote Gli1 binding to its target promoters, it has no clear effects on their epigenetic status (Fig. S9) in neural stem cells. Thus, other factors are

likely involved in the regulation of EED by RNF220, the molecular details of which require future investigation.

Together with our previous work (Ma et al., 2019), we propose RNF220 as a bivalent modulator for Shh signaling in different contexts. During ventral spinal cord patterning, RNF220 targets only Glis, including both GliA and GliR, to regulate their nuclear exportation and gradient formation. In addition to Glis, RNF220 targets EED in the CGPNs to modify the epigenetic status of Gli target genes, the effects of which override that of Gli translocation, resulting in an absolute positive role of RNF220 in Shh signaling. During Shh-group MB progression, RNF220 works in the same way as in CGPNs to amplify Shh signaling and accelerates tumorigenesis. How RNF220 is stabilized in Shh-group MB remains to be investigated..

MATERIALS AND METHODS

Animals

All mice were maintained and handled according to the guidelines approved by the Animal Care and Use Committee of the Kunming Institute of Zoology, Chinese Academy of Sciences. All mice were maintained on a C57BL/6 background. Analysis was performed only after lines were crossed to C57BL/6 for at least three generations. The following mouse lines were used, RNF220^{fl/fl}, Rosa26-CreER (008463; The Jackson Laboratory, Bar Harbor, ME), and Ptch1^{+/-} (003081; The Jackson Laboratory).

When comparing the medulloblastoma incidence in RNF220^{+/-}; Ptch1^{+/-} and Ptch1^{+/-} mice, the same aged mice of different genotypes with the same C57BL/6 background were selected and observed for a one-year long since their birth. During the observation the mice were sacrificed only when they showed some paralyzed behaviors and at the end of the observation all the remaining mice were sacrificed to assess tumor incidence.

Plasmids, cell lines, siRNAs, lentiviral preparation, infection, and stable cell line construction

RNF220 and ubiquitin expression constructs were described previously (Ma et al., 2017; Ma et al., 2019b). Mouse EED plasmid was obtained from OriGene (MR207038L1V; Rockville, MD) and then subcloned into the pCS2⁺ FLAG or myc expression vectors. HEK293, HEK293T, Shh-N HEK293T, and Daoy cells were cultured in DMEM containing 10% fetal bovine serum (FBS; Merck Millipore, Burlington, MA), 100 U/mL penicillin, and 100 mg/mL streptomycin (Life Technologies, Carlsbad, CA). Primary CGNP cultures were derived from dissociated P7 mouse cerebella and cultured in DMEM/F12 media containing 25 mM KCl, N2 supplements, and 10% FBS. For Shh stimulation, Shh-N conditional medium produced from Shh-N HEK293T cells were added at a 1:20 dilution to CGNPs. All cells were cultured in a humidified incubator with 5% CO₂ at 37°C. RNF220^{fl/fl}; Rosa26-CreER CGNPs were treated with 2 ng/mL 4-OHT for 3 days to induce RNF220 knockout.

shRNA sequences targeting human RNF220-1#: 5'-GAGCTATCAGTCAGCCTTTAC-3' and RNF220-2#: 5'-GCGTACACACACACATTTA-3' were cloned into the pLKO.1 lentiviral vector. The lentiviral DNA vectors were then co-transfected into HEK293T cells with the packaging plasmids pCMV Δ 8.9 and pMD2.G at a ratio of 10:5:2. The culture medium was collected and centrifuged at 2,500 rpm for 10 min, and the supernatant was filtered. The supernatant containing lentiviral particles was centrifuged at 25,000 rpm at 4 °C for 2.5 h. The lentivirus pellet was then re-suspended in PBS containing 0.1% bovine serum albumin (BSA) and stored at -80 °C in aliquots. The copy number of the lentiviral particles was confirmed *via* quantitative RT-PCR using the U5 primers: forward: 5'-AGCTTGCCTTGAGTGCTTCA-3' and reverse: 5'-TGACTAAAAGGGTCTGAGGG-3'. Daoy cells (5×10^5) seeded in 6-cm plates were infected at a multiplicity of infection (MOI) of 10. After infection, the cells were selected by puromycin at a concentration of 2 μ g/mL for 4–10 days to obtain stably transfected cell lines. Doxycycline (Dox; 2 μ g/mL) was used to induce shRNA expression to knockdown endogenous RNF220 in Daoy cells.

Small interfering RNAs Targeting mouse and human RNF220 and EED were synthesized as follows: mouse siRNF220-1#: 5'-CCUGCAAGAACAGCGACAUUG-3'; mouse siRNF220-2#: 5'-AGACUGAAGCACAUGUAAUUAU-3'; mouse siEED-1#: 5'-GCAGCGACGAGAACAGCAACC-3'; mouse siEED-2#:

5'-UAGUAAGGGCACAUAGAGCAU-3';	human	siRNF220-1#:
5'-GCGUACACACACACACAUUUA-3';	human	siRNF220-2#:
5'-ACUACACCUCCACCCUCAAUU-3';	human	siEED-1#:
5'-ACCCAGUGAAUCUAAUGUGAC-3';	human	siEED-2#:
5'-GUGUAGCCCAUUCCACAGACU-3'.		

Immunoprecipitation, *in vivo* ubiquitination, and western blot assays

Cells were lysed in IP buffer (50 mM Tris-HCl [pH 7.5], 150 mM NaCl, 1% Triton X-100, and Roche complete protease inhibitor cocktail [Basel, Switzerland]) and then lysates were clarified by centrifugation for 15 min at $14,000 \times g$. The protein concentration of each cell lysate sample was determined by a bicinchoninic acid (BCA) assay. Immunoprecipitation was carried out with anti-FLAG M2 beads (Sigma-Aldrich, St. Louis, MO) or the indicated antibodies coupled to protein A/G-agarose beads (Santa Cruz Biotechnology, Dallas, TX), after which the isolated proteins were subjected to SDS-PAGE followed by western blot analysis. *In vivo* ubiquitination and western blot assays were carried out as described previously (Ma et al., 2017; Ma et al., 2014). The antibodies used were anti-Gli1 (2534, 1:1000, Cell Signaling Technology, Danvers, MA), anti-RNF220 (HPA027578, 1:1000, Sigma-Aldrich, St. Louis, MO), anti-TCF4 (2569, 1:1000, Cell Signaling Technology, Danvers, MA), anti-EZH2 (A304-197A, 1:1000, Bethyl Laboratories, Montgomery TX), anti-SUZ12 (A302-407A, 1:1000, Bethyl Laboratories, Montgomery TX), anti-EED (ab4469, 1:1000, Abcam, Cambridge, UK), anti- α -tubulin (66031-1, 1:1000, Proteintech, Rosemont, IL),

anti- β -actin (ab6276, 1:5000, Abcam, Cambridge, UK), anti-FLAG (F7425, 1:5000, Simga-Aldrich, St. Louis, MO), anti-ubiquitin (sc-8071, 1:1000, Santa Cruz Biotechnology, Dallas TX) and anti-myc (C3956, 1:5000, Sigma-Aldrich, St. Louis, MO).

Chromatin immunoprecipitation (ChIP)-qPCR assays

Chromatin was cross-linked with 1% formaldehyde and cells were incubated in ChIP lysis buffer (150 mM NaCl, 25 mM Tris [pH 7.5], 1% Triton X-100, 0.1% SDS, 0.5% deoxycholate, and Roche complete protease inhibitor cocktail). The reaction was stopped by the addition of 125 mM glycine. DNA was fragmented into 200–500 bp fragments using a Bioruptor UCD-200 sonicator. Aliquots of protein lysates (400 μ g) were used for each immunoprecipitation reaction with anti-Gli1 (2534, Cell Signaling Technology, Danvers, MA), anti-IgG (sc-2027, Santa Cruz Biotechnology, Dallas TX), anti-H3K27me3 (ab192985, Abcam, Cambridge, UK), anti-H3K9me3 (ab184677, Abcam, Cambridge, UK), anti-AcH3K27 (ab4729, Abcam, Cambridge, UK), anti-AcH3K4 (ab4441, Abcam, Cambridge, UK), and anti-H3K4me3 (ab8580, Abcam, Cambridge, UK) antibodies (2 μ g). Input or precipitated genomic DNA was purified by the QIAquick PCR Purification Kit (28104; Qiagen) and used as a template for semi-quantification PCR with the following primers: mouse Gli1 promoter site 1 forward, 5'-CAGCTTAACCCACGCTGGTGAGAC-3' and reverse, 5'-ATGGTTCAGCAGTTAAGAACAAGT-3'; mouse Gli1 promoter site 2 forward, 5'-CTAGGAATTCTGGACTTCTGAGTT-3' and reverse,

5'-TCCCAAAGCTAACTGTCCTGGGTT-3'; mouse Ptch1 promoter site 1 forward,
5'-CTAAGATGTCTTAAGGACCAGCC-3' and reverse,
5'-GATAATACTTAGGCCATGTCAGC-3'; mouse Ptch1 promoter site 2 forward,
5'-TTAGAGTCATCTAGTGGCTTGAG-3' and reverse,
5'-TTGCTTAGGCTACAGTCCACCAC-3'; mouse Hhip1 promoter site 1 forward,
5'-CTTTAGGCCATCTTGCATAAGCC-3' and reverse,
5'-GGCAGGCATAGACAAATGCTGCT-3'; mouse Hhip1 promoter site 2 forward,
5'-CATTGCAAACACTGAAGTGGTCA-3' and reverse,
5'-GAATCCATGTGCTTTTAGTCATC-3'; human Gli1 promoter site 1 forward,
5'-CATTATTGATAAGTAAGGACTTAC-3' and reverse,
5'-AAGTCAGAGAATGAAGTTAAGGTG-3'; human Gli1 promoter site 2 forward,
5'-CACACCAGTTAGAATGGCAATCAT-3' and reverse,
5'-GCAGTGGCACGATCTCAGCTCAC-3'; human Ptch1 promoter site 1 forward,
5'-CAAGCCCTACATGTAGTTAACCAG-3' and reverse,
5'-GACTGTCCTACCACACTCTGAGCA-3'; human Ptch1 promoter site 2 forward,
5'-GATAGGCATTTGTAAGTGTGCTG-3' and reverse,
5'-TCTCAGACGTCTTGCACCTAAGTC-3'; human Hhip1 promoter site 1 forward,
5'-AGACTTGAACAATGCTATCTACTA-3' and reverse,
5'-TCTAATCCCTCCTTTAAGTTCTTC-3' and human Hhip1 promoter site 2
forward, 5'-GCAATATTTAAGAGGTACTATGCA-3' and reverse,
5'-CAACCTCCATCTCCCAGGTTCAAG-3'.

RNA isolation, reverse transcription, and real-time PCR

Total RNA was isolated from tissues or cells using TRIzol reagent (Thermo Fisher Scientific, Waltham, MA) according to manufacturer's instructions. For each sample, about 1 µg RNA was reverse-transcribed to cDNA using a first strand cDNA synthesis kit (Fermentas, Waltham, MA). Gene expression was quantified using LightCycler 480 SYBR Green I Master (Roche) and a LightCycler 480 system (Roche). All reactions were run in at least triplicate. The following primers were used: mouse RNF220 forward, 5'-TGTGGGCAGAAGCGGATAC-3' and reverse, 5'-TGTCATCTCCATCCACATCCAG-3'; mouse Gli1 forward, 5'-GGAGACAGCATGGCTCACTA-3' and reverse, 5'-GAGGTTGGGATGAAGAAGCA-3'; mouse Ptch1 forward, 5'-CCCTAACAAAATTCAACCAAACCT-3' and reverse, 5'-GCATATACTTCCTGGATAAACCTTGAC-3'; mouse Hhip1 forward, 5'-GGAGTAACCCTCACTTCAACAGCA-3' and reverse, 5'-CCCGTTGGAATCTGAGCAAAGTA-3'; mouse EED forward, 5'-GAGCAGCGACGAGAACAGCAACC-3' and reverse, 5'-ATTTGGCGTATTTGTGGGCGTGT-3'; mouse β-actin forward, 5'-TGAGCGCAAGTACTCTGTGTGGAT-3' and reverse, 5'-ACTCATCGTACTCCTGCTTGCTGA-3'; human RNF220 forward, 5'-GATGCCATCCACCAGCAA-3' and reverse, 5'-CACGAGATAGCTGCCGTTCA-3'; human Gli1 forward,

5'-TGTGTATGAAACTGACTGCCG-3' and reverse,
 5'-CCCAGTGGCACACGAACTC-3'; human Ptch1 forward,
 5'-TGTGCGCTGTCTTCCTTCTG-3' and reverse,
 5'-CACGGCACTGAGCTTGATTC-3'; human Hhip1 forward,
 5'-ATTGCTTCCCTAATGTCCT-3' and reverse,
 5'-GGGAGGTAGACCCACACCA-3'; human EED forward,
 5'-GTGACGAGAACAGCAATCCAG-3' and reverse,
 5'--TATCAGGGCGTTCAGTGTTG-3'; human β -actin forward,
 5'-ACCGAGCGCGGCTACAG-3' and reverse,
 5'-CTTAATGTCACGCACGATTCC-3'.

Immunofluorescence staining

CGNPs or Daoy cells or sections were fixed with 4% paraformaldehyde for 20 min after washing in PBS. After permeabilization with 0.5% Triton X-100 and blocking with 3% BSA, cells were incubated overnight at 4 °C with primary antibody and further stained with a Cy3 or FITC-conjugated secondary antibody for 2 h in the dark at room temperature. The primary antibodies were used as follows: RNF220 (HPA027578, 1:200, Simga-Aldrich, St. Louis, MO); NeuN (MAB377, 1:400, Simga-Aldrich, St. Louis, MO) and Ki67 (ab15580, 1:200, Abcam, Cambridge, UK). Cells or sections were then incubated with 4-6-diamidino-2-phenylindole (DAPI) for 1 min to counterstain nuclei. Fluorescence was imaged by laser confocal scanning microscopy (Olympus, Tokyo, Japan).

Soft agar colony formation assays

Complete medium containing 0.6% agarose (Sigma-Aldrich, St. Louis, MO) was mixed by pipetting and then aliquoted at 1 mL/well in a 6-well plate. Next, the plates were cooled for approximately 5 min at 4 °C to solidify the agarose (base agar). A total of 2×10^4 cells were mixed with 1 mL complete medium containing 0.3% soft agar and added on top of the base agar. Then, the plates were cooled again for approximately 5 min at 4 °C. Thereafter, 1 mL complete medium was added to each well. After 4 weeks, 1 mL PBS containing 4% formaldehyde and 0.005% crystal violet were added to fix and stain the colonies.

Xenograft mouse model

A total of 2×10^6 Daoy cells resuspended in PBS were subcutaneously injected into 3-week-old BALB/c nude mice. Dox was incorporated with the food when the cells were injected. The number of mice *per* group was six. The tumor volume was calculated by the formula $0.5 \times \text{length} \times \text{width}^2$, and the data were represented as the mean \pm SEM.

Bromodeoxyuridine (BrdU) incorporation assay

For BrdU pulse labeling experiments to analyze cell proliferation, pregnant mice or mouse pups were injected with BrdU at 100 mg/kg bodyweight and brains were dissected for analysis 2 hours later. Tissue sections were immersed in 0.01 M citrate buffer at 95°C for 5 min, 2 M HCl at 37°C for 20 min, 0.1 M sodium borate for 10 min, and then washed in PBS. For CGNP or Daoy cells labeling, BrdU was added to the

cell medium at a final concentration of 10 μ M and incubated for 1 h. Cells were then fixed with 4% paraformaldehyde in PBS followed by permeabilization with 0.3% Triton X-100 in PBS. Thereafter, the cells were treated with 2 M HCl for 30 min and blocked with 10% goat serum in a PBS solution for 1 h at room temperature. Treated sections or cells were immunostained with anti-BrdU (OBT0030G, 1:200, Bio-Rad Laboratories, Hercules, CA) antibody, followed by incubation with the Cy3-labeled secondary antibody. Sections were observed and images were captured using an epifluorescence microscope (IX73, Olympus).

MTS assay

Daoy cells (2×10^5) seeded in 6-well plates were incubated with or without 2 μ g/mL Dox. After 4 days of treatment, the cells were trypsinized and seeded in 96-well plates at a density of 2×10^3 cells/well. The residual cells were collected for western blotting and RT-PCR to determine RNF220 expression. MTS (20 μ L; Promega, Madison, WI) was added to each sample at the indicated time point, and the cells were then incubated at 37 °C for 1 h. Finally, the OD value was measured at 492 nm using a microplate reader (Bio-Rad Laboratories, Hercules, CA). The data are represented as the mean \pm SD (n = 6).

Paraffin sectioning and immunohistochemical staining

Mice were anesthetized with 10% chloral hydrate and perfused through the ascending aorta with 150 mL normal saline (0–4 °C) followed by 200 mL of 4% paraformaldehyde (0–4 °C). The brain was removed and the cerebellum was isolated, fixed in 10% formalin, and embedded in paraffin as previously described (Ma et al., 2019a; Ma et al., 2019b). Sections (10 µm thick) were cut and subjected to immunofluorescence staining as previously described (Ma et al., 2019a; Ma et al., 2019b). Immunohistochemistry on clinical MB tissue array samples (BC17012; Alenabio, Xi'an, China) was performed. There are 32 independent human medulloblastoma cases with two samples for each case on the slide. The array samples were subjected to GAB1 staining to distinguish Shh and other subgroups of MBs. RNF220 (HPA027578, 1:200; Sigma-Aldrich, St. Louis, MO) and GAB1 (GTX111253, 1:50; GeneTex, Irvine, CA) antibodies were used. Chromogen development was performed with the DAB detection kit (Beyotime Institute of Biotechnology, Jiangsu, China) according to manufacturer's instructions. The percentage of positive cells and staining intensity were multiplied to produce a weighted score for each case.

Statistical analysis

Each experiment was conducted at least three times with the same results. Data were analyzed using the GraphPad software as follows: 1) For experiments including qRT-PCR, colony formation and BrdU/Ki-67 staining, statistical significance was evaluated using the two-tailed student's *t*-test for comparison of 2 groups; 2) For associations between gene expression values, significance was evaluated by Pearson product-moment correlation coefficient analysis. Image J software was used to quantify the Western Blot data. CellSens software equipped with Olympus IX73 microscope were used for cerebellum size quantification. The cerebellum EGL length was normalized to bodyweight.

ACKNOWLEDGEMENTS

This work was supported by grants from the National Natural Science Foundation of China (31500847 to P.M; 81773783 to Y.L; 31671521 and U1302226 to B.M) and the open project of State Key Laboratory of Genetic Resources and Evolution (GREKF18-12 to Y.L).

AUTHOR CONTRIBUTIONS

B. Mao and Y. Li conceived and designed the project; P. Ma and T. An carried out most of the experiments; L. Zhang counted cells for BrdU and Ki-67 staining; B. Ren and H. Wang performed the biochemical assays; B. Sun and X. Zhou constructed the stable cell lines; L. Zhu performed paraffin sectioning and immunohistochemical staining; and P. Ma, T. An, Y. Li, and B. Mao wrote the manuscript.

COMPLIANCE WITH ETHICS GUIDELINES

The authors declare that they have no conflict of interest.

REFERENCES

- Briscoe J, Therond PP (2013) The mechanisms of Hedgehog signalling and its roles in development and disease. *Nat Rev Mol Cell Biol* 14:416-429
- Fuccillo M, Joyner AL, Fishell G. (2006) Morphogen to mitogen: the multiple roles of hedgehog signalling in vertebrate neural development. *Nat Rev Neurosci* 7:772-783
- Gajjar AJ, Robinson GW (2014) Medulloblastoma—translating discoveries from the bench to the bedside. *Nature Reviews Clinical Oncology* 11:714
- Hui CC, Angers S (2011) Gli proteins in development and disease. *Annu Rev Cell Dev Biol* 27:513-537
- Ingham PW, Placzek, M (2006) Orchestrating ontogenesis: variations on a theme by sonic hedgehog. *Nat Rev Genet* 7:841-850
- Ivanov DP, Coyle B, Walker DA, Grabowska AM (2016) In vitro models of medulloblastoma: Choosing the right tool for the job. *J Biotechnol* 236:10-25
- Kim YJ, Osborn DP, Lee JY, Araki M, Araki K, Mohun T, Kansakoski J, Brandstack N, Kim HT, Miralles F et al. (2018) WDR11-mediated Hedgehog signalling defects underlie a new ciliopathy related to Kallmann syndrome. *EMBO Rep* 19:269-289
- Lanzuolo C, Orlando V (2012) Memories from the Polycomb Group Proteins. *Annual Review of Genetics* 46:561-589
- Lisa V Goodrich LM, Kay M Higgins, Matthew P Scott (1997) Altered Neural Cell Fates and Medulloblastoma in Mouse patched Mutants. *Science* 277 (5923):1109-1113
- Louis DN, Perry A, Reifenberger G, von Deimling A, Figarella-Branger D, Cavenee WK, Ohgaki H, Wiestler OD, Kleihues P, Ellison DW (2016) The 2016 World Health Organization Classification of Tumors of the Central Nervous System: a summary. *Acta Neuropathologica* 131:803-820
- Ma P, Ren B, Yang X, Sun B, Liu X, Kong Q, Li C, Mao B (2017) ZC4H2 stabilizes Smads to enhance BMP signalling, which is involved in neural development in *Xenopus*. *Open Biol* 7

Ma P, Song NN, Cheng X, Zhu L, Zhang Q, Zhang L, Yang X, Wang H, Kong Q, Shi D et al. (2019a). ZC4H2 stabilizes RNF220 to pattern ventral spinal cord through modulating Shh/Gli signaling. *J Mol Cell Biol*

Ma P, Song NN, Li Y, Zhang Q, Zhang L, KongQ, Ma L, Yang X, Ren B, Li C et al. (2019b). Fine-Tuning of Shh/Gli Signaling Gradient by Non-proteolytic Ubiquitination during Neural Patterning. *Cell Rep* 28:541-553 e544.

Ma P, Yang X, Kong Q, Li C, Yang S, Li Y, Mao B (2014) The ubiquitin ligase RNF220 enhances canonical Wnt signaling through USP7-mediated deubiquitination of beta-catenin. *Mol Cell Biol* 34:4355-4366

Malatesta M, Steinhauer C, Mohammad F, Pandey DP, Squatrito M, Helin K (2013) Histone acetyltransferase PCAF is required for Hedgehog-Gli-dependent transcription and cancer cell proliferation. *Cancer Res* 73:6323-6333

Northcott PA, Buchhalter I, Morrissy AS, Hovestadt V, Weischenfeldt J, Ehrenberger T, Grobner S, Segura-Wang M, Zichner T, Rudneva V.A et al. (2017). The whole-genome landscape of medulloblastoma subtypes. *Nature* 547:311-317

Northcott PA, Jones DT, Kool M, Robinson GW, Gilbertson RJ, Cho YJ, Pomeroy SL, Korshunov A, Lichter P, Taylor MD et al. (2012) Medulloblastomics: the end of the beginning. *Nat Rev Cancer* 12:818-834

Pasca di Magliano M, Hebrok M (2003) Hedgehog signalling in cancer formation and maintenance. *Nat Rev Cancer* 3:903-911

Quaranta R, Pellulo M, Zema S, Nardoza F, Checquolo S, Lauer DM, Bufalieri F, Palermo R, Felli MP, Vacca A et al. (2017) Maml1 acts cooperatively with Gli proteins to regulate sonic hedgehog signaling pathway. *Cell Death Dis* 8, e2942.

Ruiz i Altaba A, Palma V, Dahmane N (2002) Hedgehog-Gli signalling and the growth of the brain. *Nat Rev Neurosci* 3:24-33

Shi X, Zhang Z, Zhan X, Cao M, Satoh T, Akira S, Shpargel K, Magnuson T, Li Q, Wang R et al. (2014) An epigenetic switch induced by Shh signalling regulates gene activation during development and medulloblastoma growth. *Nat Commun* 5:5425

Song NN, Ma P, Zhang Q, Zhang L, Wang H, Zhang L, Zhu L, He CH, Mao B and Ding YQ (2020) RNF220/ZC4H2 mediated monoubiquitination of Phox2 is required for noradrenergic neuron development. *Development*: dev.185199

Vaillant C, Monard D (2009) SHH pathway and cerebellar development. *Cerebellum* 8:291-301

Wang VY, Zoghbi HY (2001). Genetic regulation of cerebellar development. *Nature Reviews Neuroscience* 2:484

Zhang Y, Wang T, Wang S, Xiong Y, Zhang R, Zhang X, Zhao J, Yang AG, Wang L, Jia L (2018) Nkx2-2as Suppression Contributes to the Pathogenesis of Sonic Hedgehog Medulloblastoma. *Cancer Res* 78:962-973

Figures

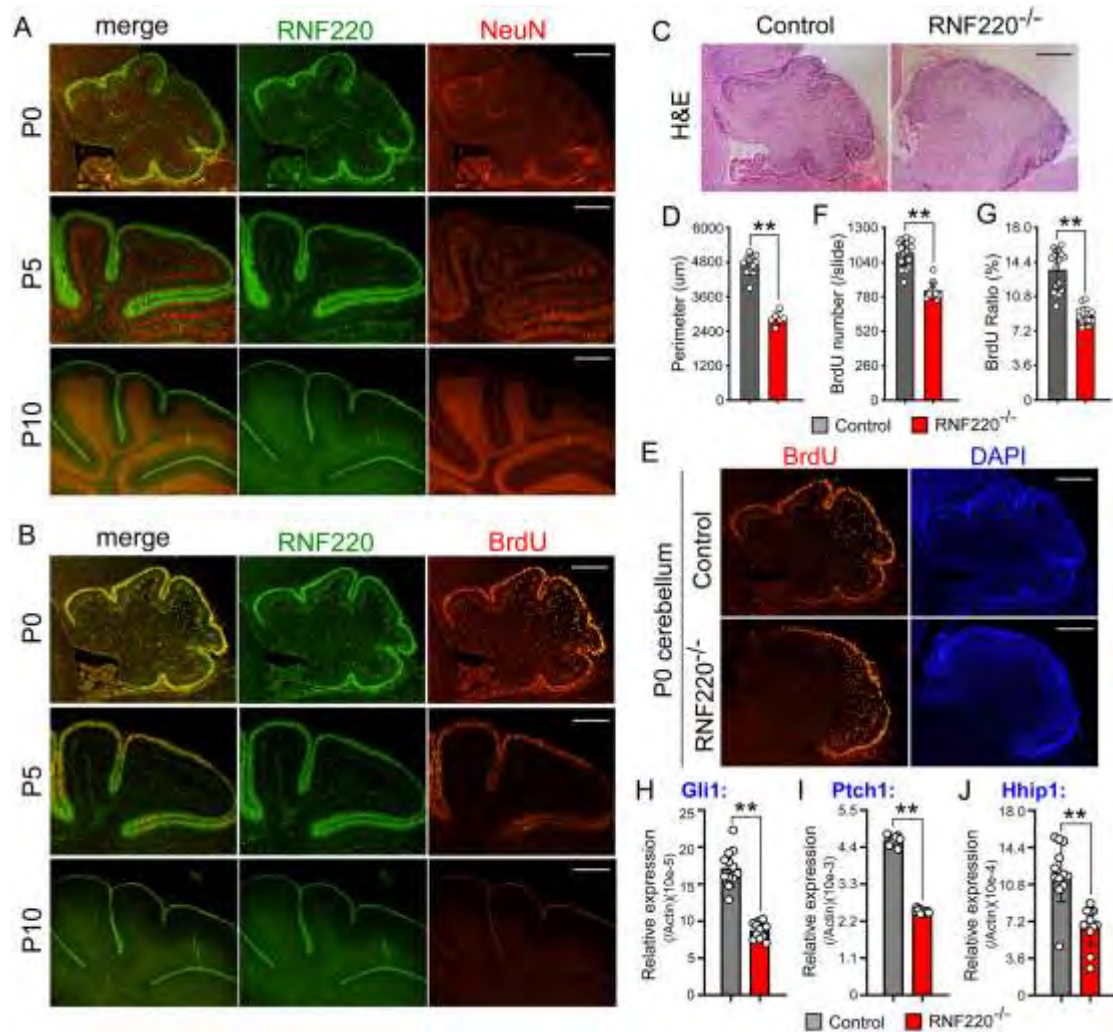


Figure 1. RNF220 is expressed at the EGL and is required for normal cerebellum development. (A) Co-staining immunofluorescence assay shows RNF220 and NeuN expression in cerebellum at different developmental stages. Scar bar, 170 μm for upper panels; 350 μm for middle panels and 940 μm for the lower panels. (B) RNF220 and BrdU co-staining immunofluorescence assay in cerebellum at different developmental stages. Scar bar, 170 μm . (C and D) Hematoxylin and eosin (H&E) staining of E19.5 control and RNF220 knockout in cerebellum midsagittal sections (C); Scar bar, 170 μm for upper panels; 350 μm for middle panels and 940 μm for the lower panels.

Quantitative analysis of the cerebellar perimeter of midsagittal cerebella sections (D).
(E-G) BrdU incorporation assay to evaluate cell proliferation in control and RNF220 knockout P0 cerebellum. Scar bar, 170 μ m. Quantification of BrdU assay results (E).
(H-J) Real-time PCR of Gli1 (H), Ptch1 (G) and Hhip1 (J) relative expression levels in control and RNF220 knockout P0 cerebellum. Data are presented as the means \pm SD.
** $p < 0.01$.

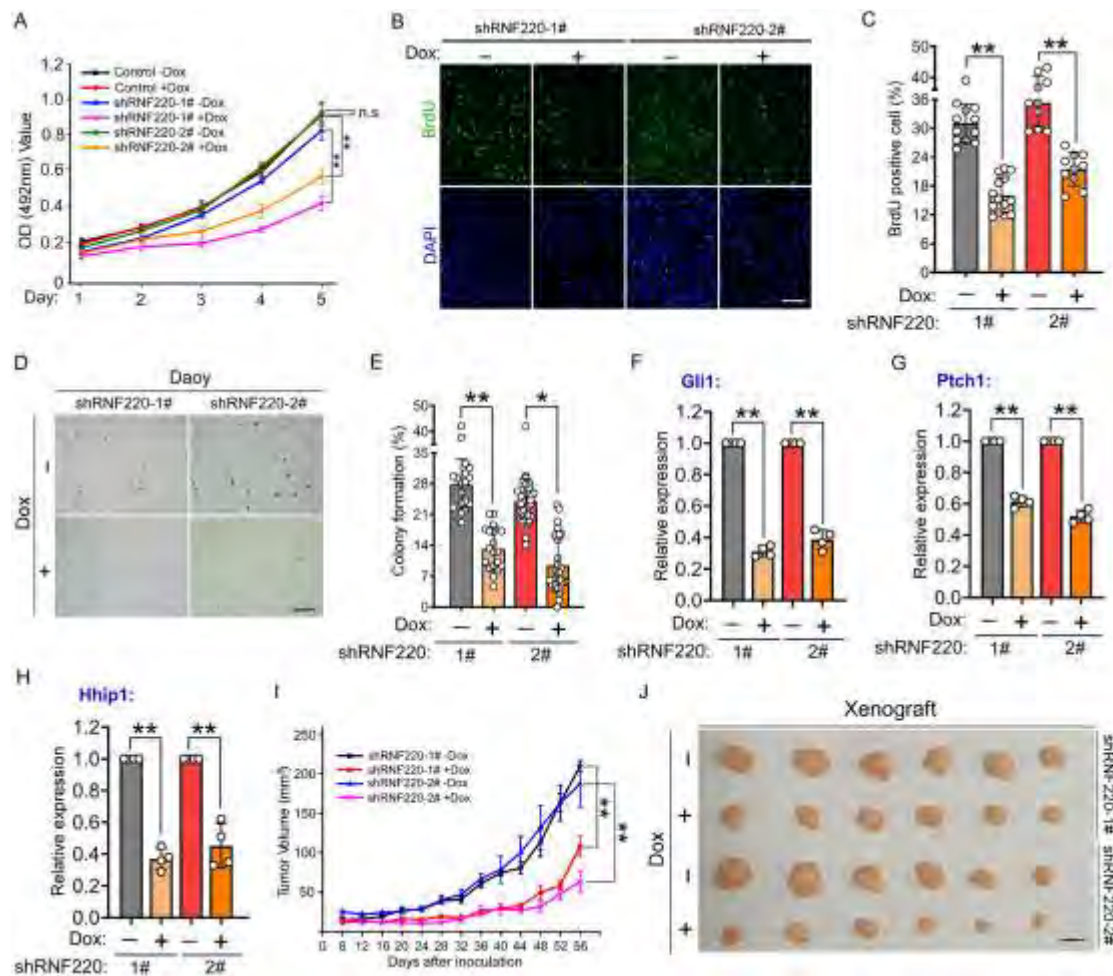


Figure 2. RNF220 is required for Daoy cell proliferation and xenograft growth.

(A) Growth curve for control and RNF220 knockdown Daoy cell lines. Dox was used to induce RNF220 knockdown in shRNF220-1# or 2# stable cell lines. (B and C) BrdU incorporation assay to evaluate DNA synthesis and proliferation rates of Daoy cells when RNF220 was knocked down by Dox induction or not. Scale bar, 50 μ m. Quantification of BrdU assay results (C). (D and E) Soft agar colony formation assays using shRNF220-1# or 2# Daoy cell clones with or without Dox. Quantification of colony number (E). Scale bar, 120 μ m. (F-H) Real-time PCR for the relative expression levels of Gli1 (F), Ptch1 (G) and Hhip1 (H) in RNF220 knockdown Daoy cell lines. (I)

shRNF220-1# or -2# clone was injected subcutaneously into BALB/c nude mice and the mice were fed with food spiked with or without Dox. Tumor size was measured every four days. The results are presented as the mean \pm SEM (n = 6). (J) Photographs of xenograft tumors from BALB/c nude mice subcutaneously injected with shRNF220-1# or 2# clone fed with or without Dox 56 days after injection. Scale bar, 0.5 cm. * $p < 0.05$; ** $p < 0.01$.

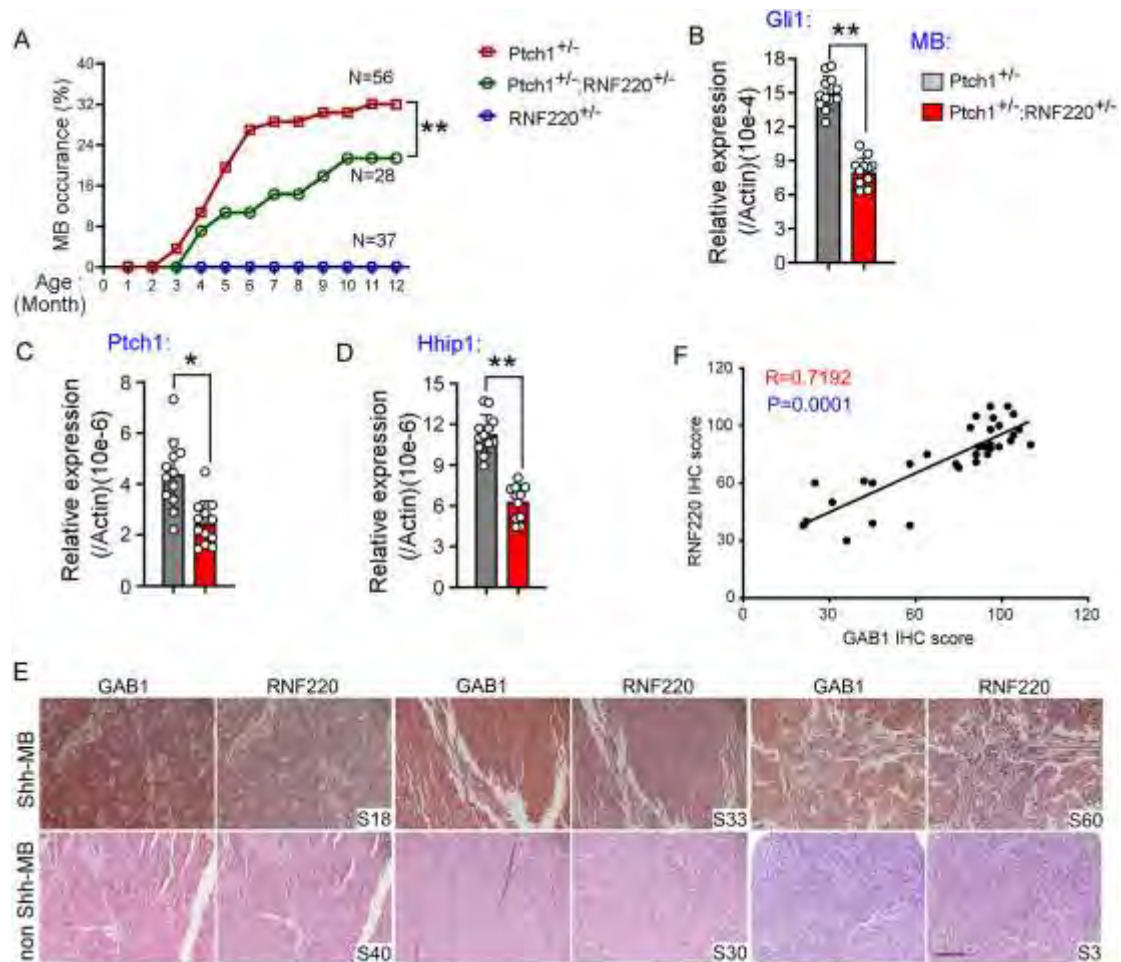


Figure 3. RNF220 is required for Shh-group MB progression. (A) Cumulative medulloblastoma occurrence of indicated mouse during 12 months observation. (B-D) Realtime PCR assays show the relative expression level of Gli1 (B), Ptch1 (C) and Hhip1 (D) in medulloblastoma tissues with different origins. (E) Representative immunohistochemical images of clinical Shh (upper panel) and non-Shh (lower panel) MB samples. Scale bar, 400 μ m. (F) Statistics analysis of the correlation between GAB1 and RNF220 based on the immunohistochemical staining scores. * $p < 0.05$; ** $p < 0.01$.

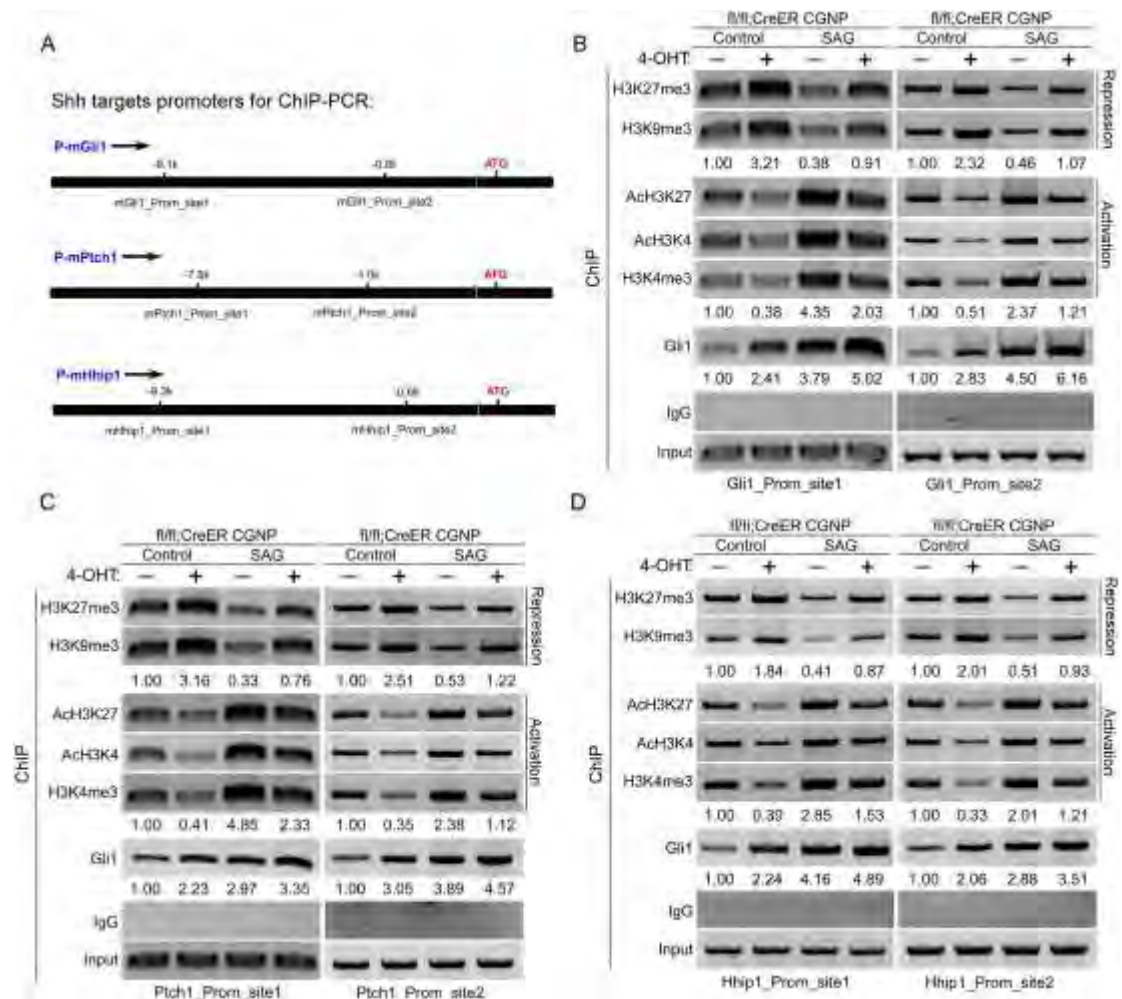


Figure 4. RNF220 regulates Shh signaling through an epigenetic mechanism in CGNPs . (A) Schematic representation of the tested Gli binding sites in mouse Gli1, Ptch1 and Hhip1 promoters. The coordinates refer to the translational start codon. (B-D) semi-quantification ChIP-PCR analysis of the indicated histone modification marks at the Gli binding sites in Gli1 (B), Ptch1 (C) and Hhip1 (D) promoters in CGNPs. CGNPs were treated with SAG or DMSO for 24 h before cells were harvested. 4-OHT was used to induce RNF220 knockout in CGNPs. Cells were harvested and followed by nuclear purification, chromosome fragments and immuniprecipitation with the indicated antibodies. PCR products from immunoprecipitated DNA were quantified

against those from inputs DNA followed by each control and the quantified data were shown below the indicated bands. Note that to make the figure concise, for each repressive or activating group, the averaged relative levels of the different marks were shown, which always changed in the same direction.

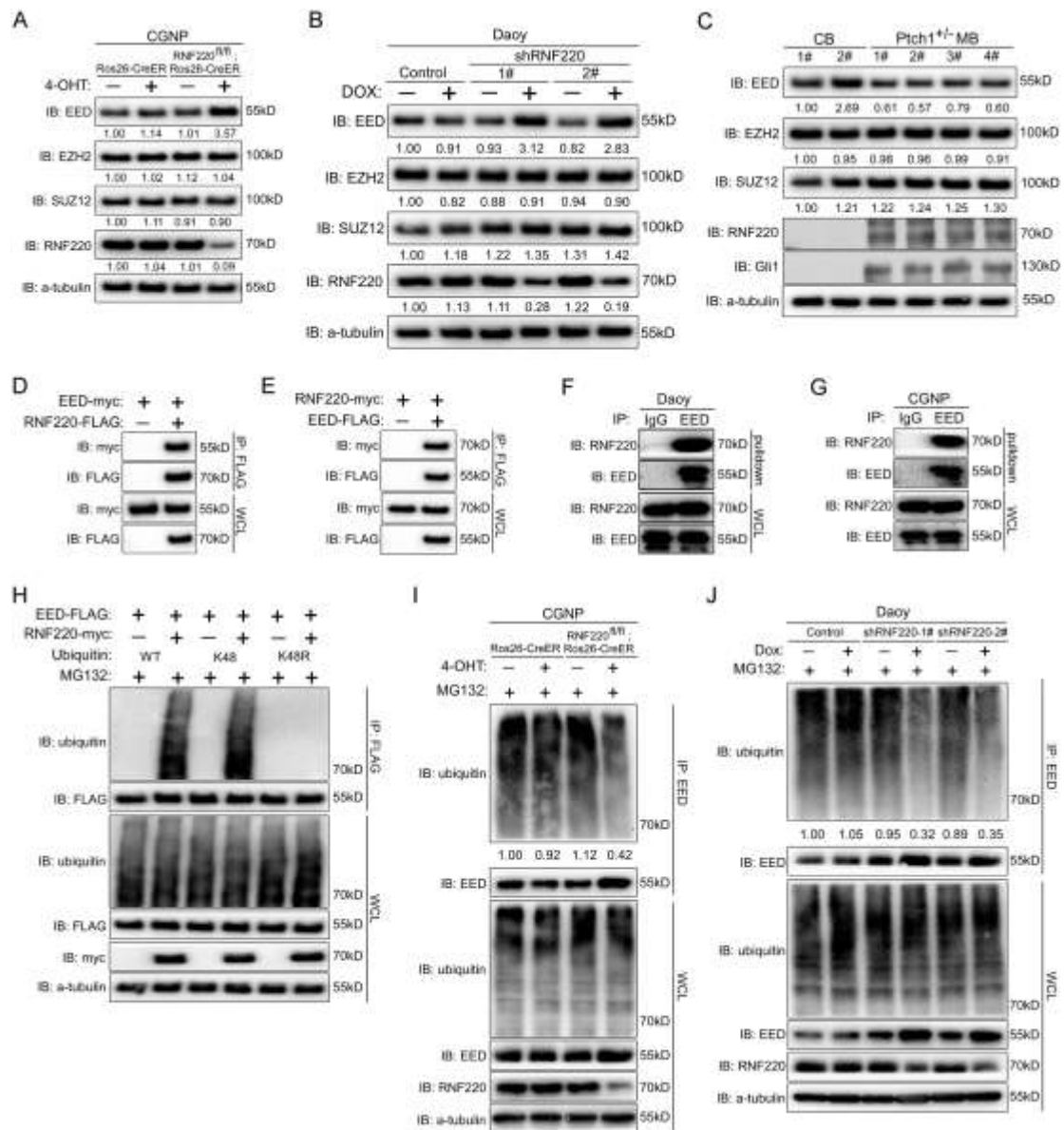


Figure 5. RNF220 interacts with and targets EED for K48-linked polyubiquitination. (A) Western blots of the indicated protein levels in CGNPs when RNF220 was knocked out or not. 4-OHT was used to knockout RNF220 in CGNP cells. (B) Western blots analysis of the effect of RNF220 knockdown on the indicated protein levels in Daoy cells. (C) Western blots of the indicated protein levels in control

cerebellum and *Ptch1*^{+/-} MB tissues. (D and E) Co-IP assays showing the interaction between RNF220 and EED proteins. HEK293 cells were transiently transfected with different combinations of RNF220 and EED expression vectors, as indicated. Cell lysates were incubated with anti-FLAG beads, washed, and subsequently analyzed by western blotting. (F and G) Endogenous RNF220 was pulled down by EED in both Daoy (F) and CGNP (G) cells. (H) *In vivo* ubiquitination assays showing the ability of RNF220 to ubiquitinate EED when the indicated ubiquitin mutant constructs were used. RNF220 promotes K48-linked polyubiquitination of EED. WT, wild-type. K48R, the K48 of ubiquitin was mutated to arginine (R); K48, ubiquitin mutants with all lysines except K48 mutated to arginine. (I and J) The ubiquitination level of endogenous EED reduced when RNF220 was knocked out in CGNPs (I) or knocked down in Daoy (J) cells. Some of protein levels were quantified against α -tubulin followed by each control and the statistics were shown below the indicated panel. IB, immunoblot; WCL, whole cell lysate; IP, immunoprecipitation.

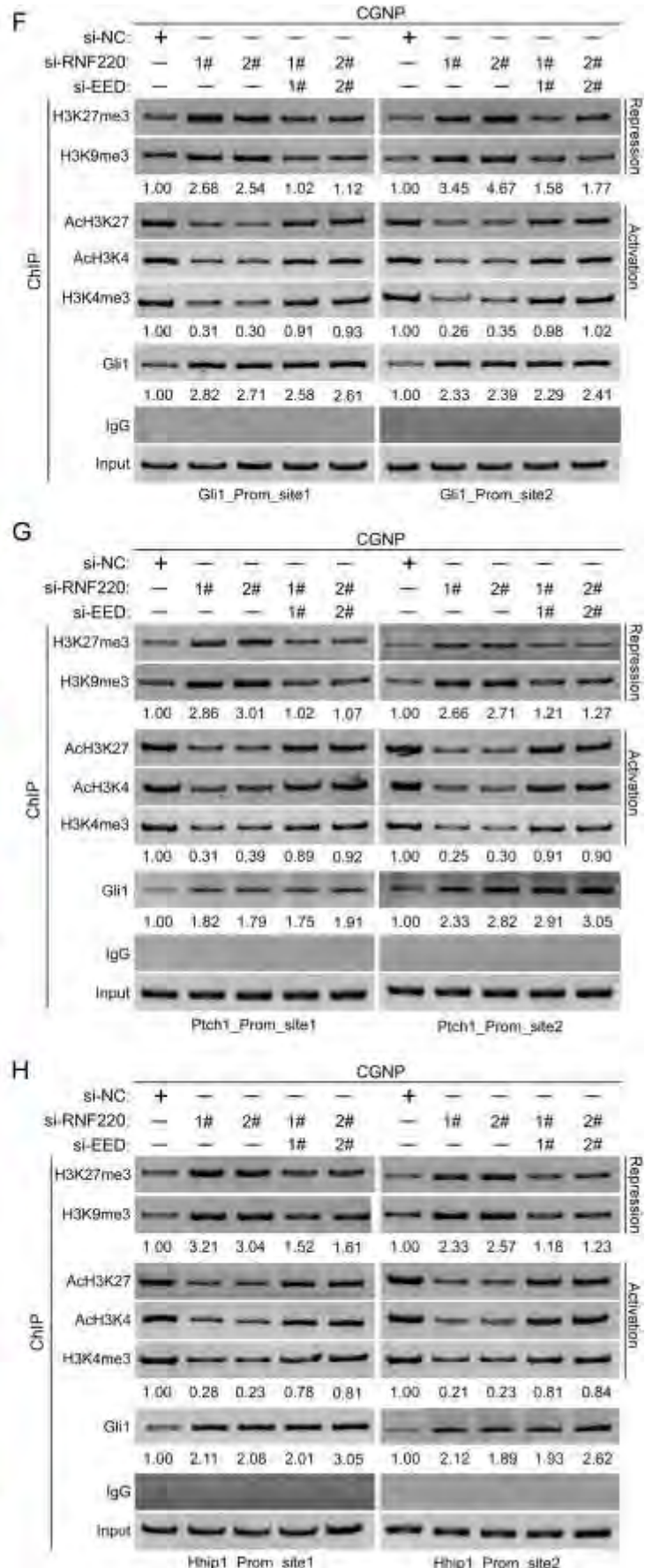
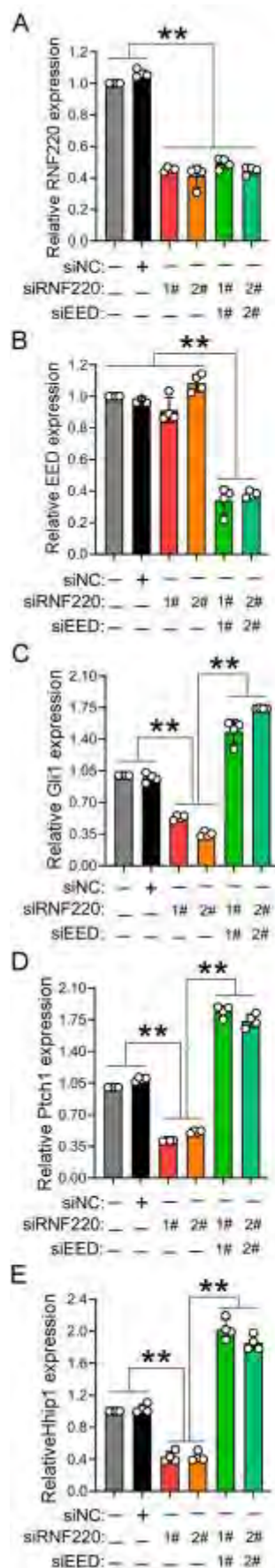


Figure 6. EED knockdown rescue RNF220 knockdown mediated Shh signaling repression and epigenetic modification changes on the promoters of Shh signaling targets in CGNPs. (A-E) Realtime PCR assays showed the relative expression level of RNF220 (A), EED (B), Gli1 (C), Ptch1 (D) and Hhip1 (E) when the indicated siRNAs were transfected into the CGNPs. (F-H) Semi-quantification ChIP-PCR analysis of histone modification marks at the indicated Gli binding sites in Gli1(F), Ptch1 (G) and Hhip1 (H) promoters in CGNPs. Cells were harvested at 72 hours after siRNAs transfection and processed for chromatin immunoprecipitation and PCR. Note that for each repressive or activating group, the averaged relative levels of the different marks were shown.. ** $p < 0.01$.

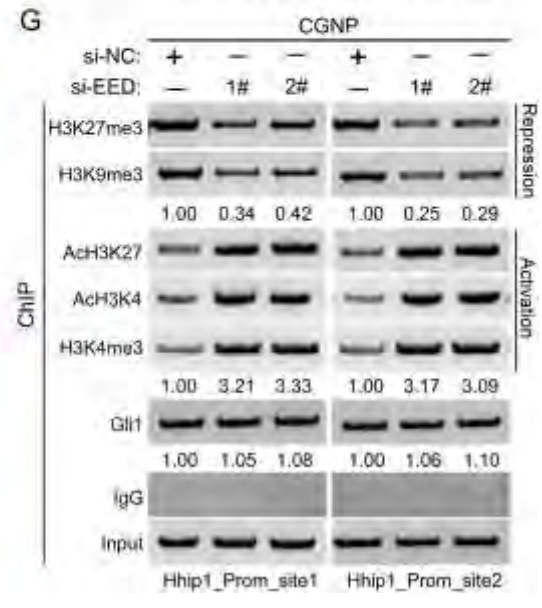
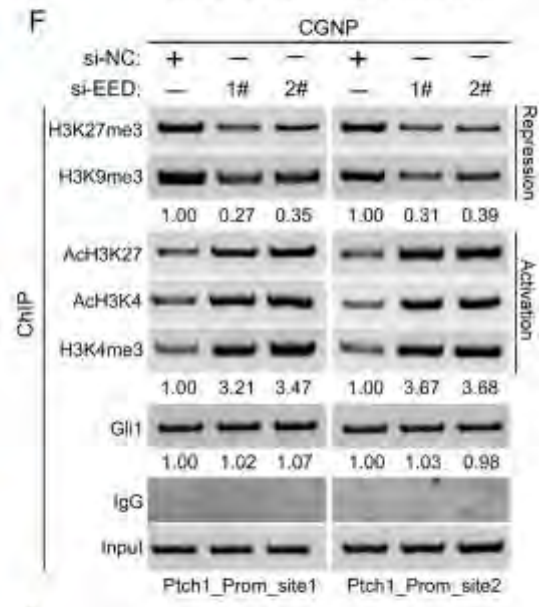
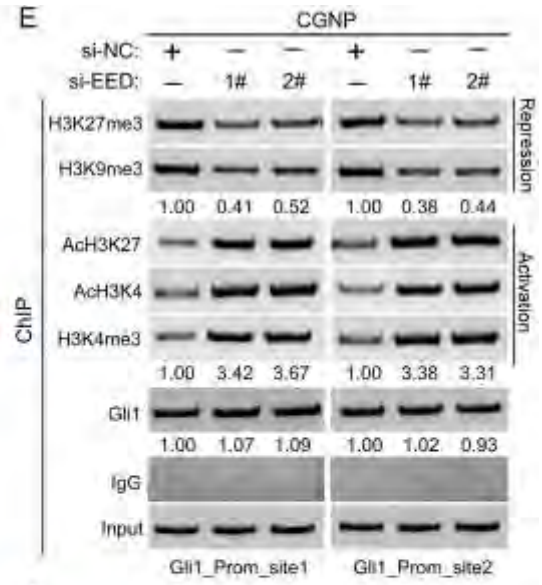
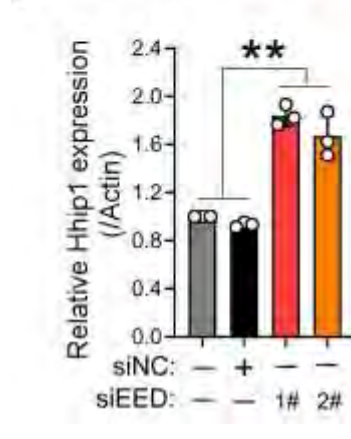
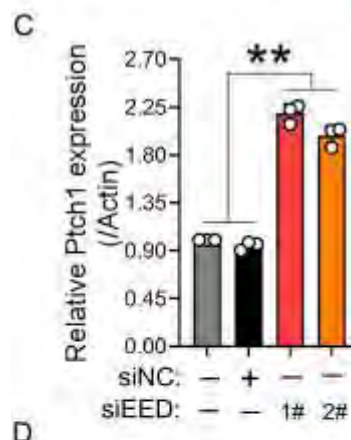
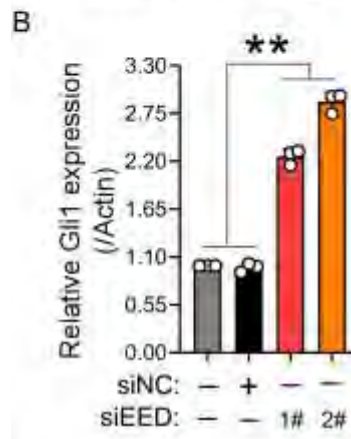
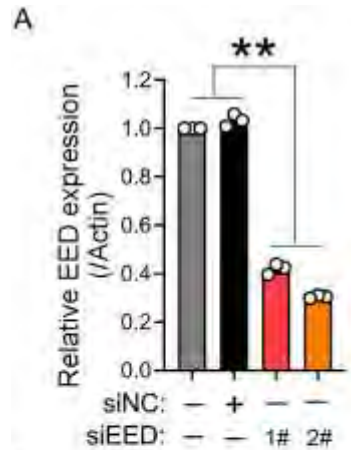


Figure 7. EED knockdown inhibits Shh signaling and changes the epigenetic modification on the promoters of Shh signaling targets in CGNPs. (A-D)

Realtime PCR assays showed the relative expression level of EED (A), Gli1 (B), Ptch1 (C) and Hhip1 (D) when the endogenous EED was knocked down in CGNPs.

(E-G) Semi-quantification ChIP-PCR analysis of histone modification marks at the indicated Gli binding sites in Gli1 (E), Ptch1 (F) and Hhip1 (G) promoters in CGNPs when endogenous EED was knocked down. Note that for each repressive or activating group, the averaged relative levels of the different marks were shown. ** $p < 0.01$.

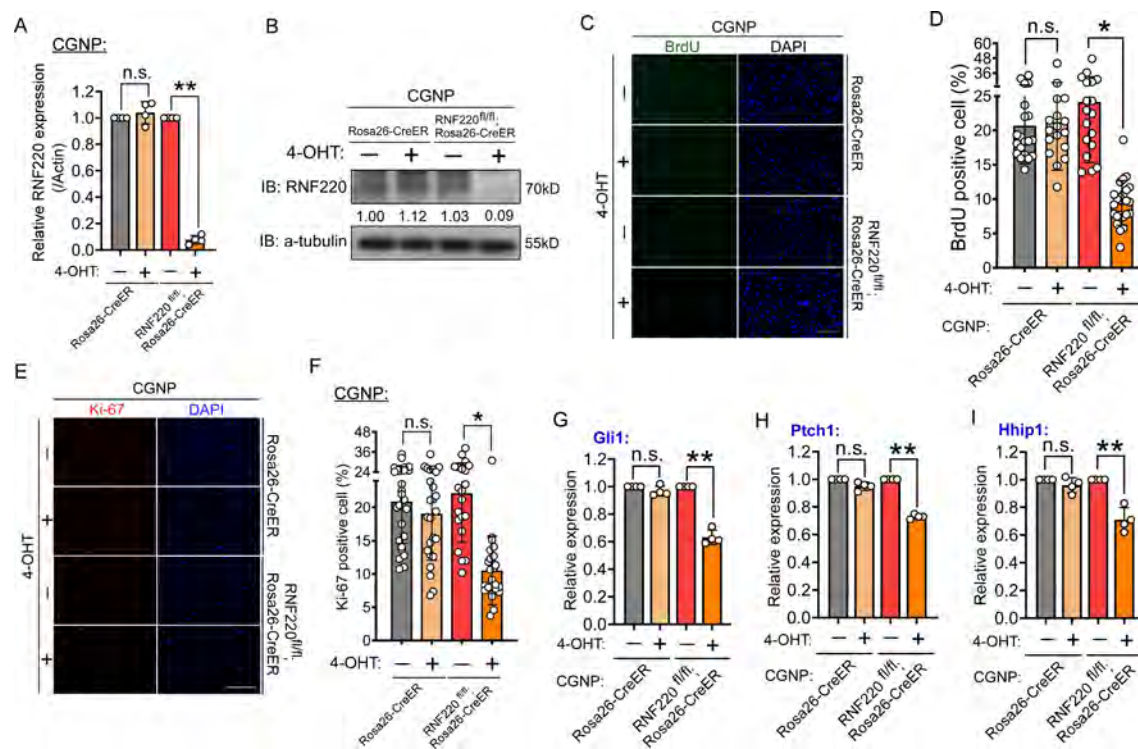


Figure S1. RNF220 knockout inhibits CGNP proliferation. (A and

B) Real-time PCR (A) and western blotting (B) showing the 4-OHT induced RNF220 knockout efficiency in CGNP cells. IB, immunoblot. (C-F) BrdU incorporation (C and D) and Ki-67 (E and F) staining assays to evaluate DNA synthesis and proliferation rates of CGNPs when RNF220 was knocked out by 4-OHT induction. Scale bar, 80 μ m. Quantification were shown in (D) and (E) respectively. (G-I) Realtime PCR assays show the relative expression level of Gli1(G), Ptch1 (H) and Hhip1 (I) in CGNP cells when RNF220 knock out was induced by 4-OHT incubation or not. Data are presented as the means \pm SD. n.s., no significant difference; * $p < 0.05$; ** $p < 0.01$.

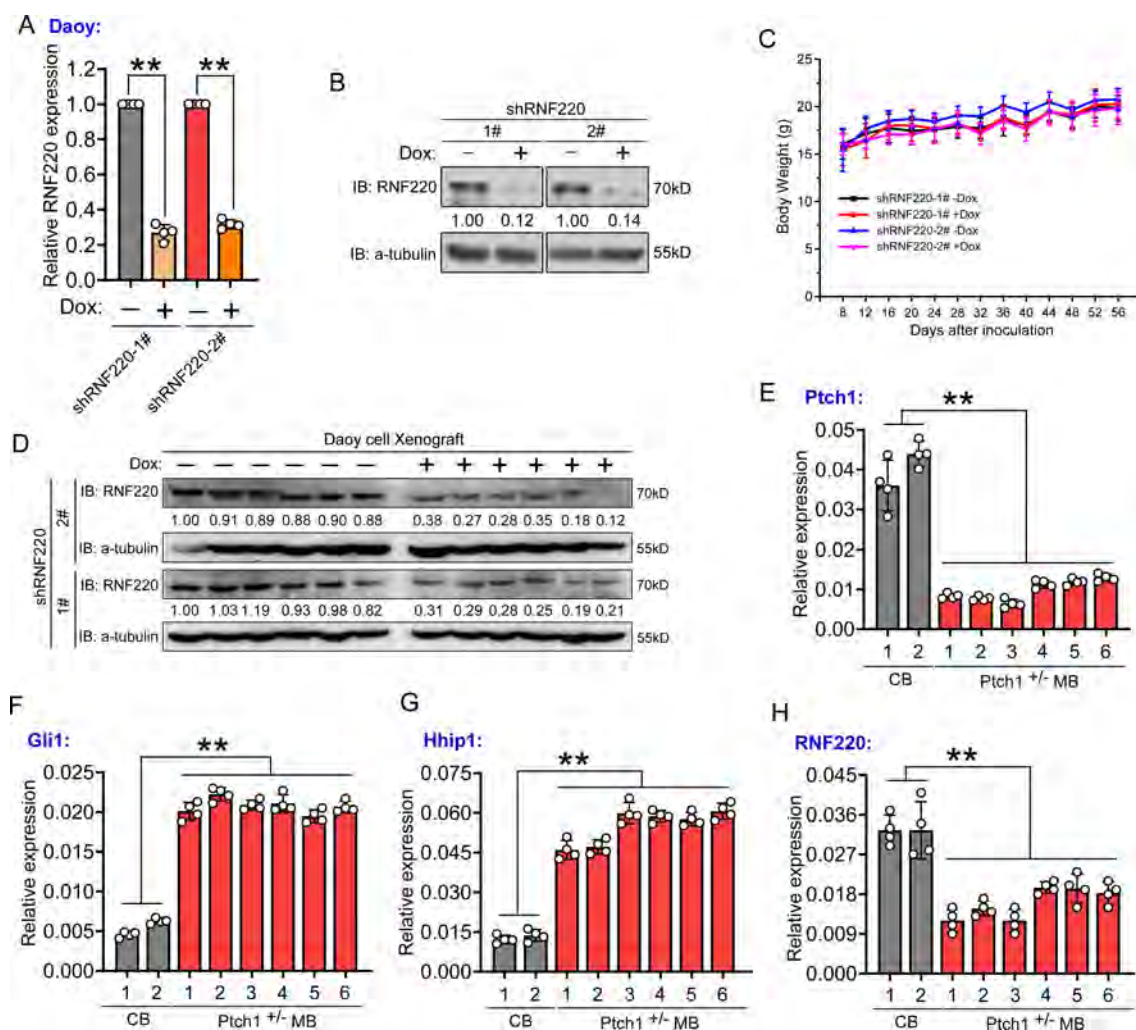


Figure S2. RNF220 knockdown efficiency and mRNA levels of Gli1,

Ptch1, Hhip1 and RNF220 in Ptch1^{+/-} MB tissues. (A and B) Real-time PCR (A) and

western blotting (B) showing the Dox-induced RNF220 knockdown efficiency in

shRNF220-1# or 2# stable Daoy cell lines. (C) Mice body weight was measured every

four days after shRNF220-1# or 2# clones were injected subcutaneously into BALB/c

nude mice and mice were fed with or without Dox. (D) RNF220 protein levels in

tumor tissues were detected by western blotting. The protein level was quantified

against α -tubulin followed by each control and the statistics were shown below each

panel. IB, immunoblot. (E–H) Real-time PCR of the relative expression of Ptch1 (E),

Gli1 (F), Hhip1 (G) and RNF220 (H) in control cerebellum and Ptch1^{+/-} MB tissues.

Data are presented as the means \pm SD. ** $p < 0.01$.

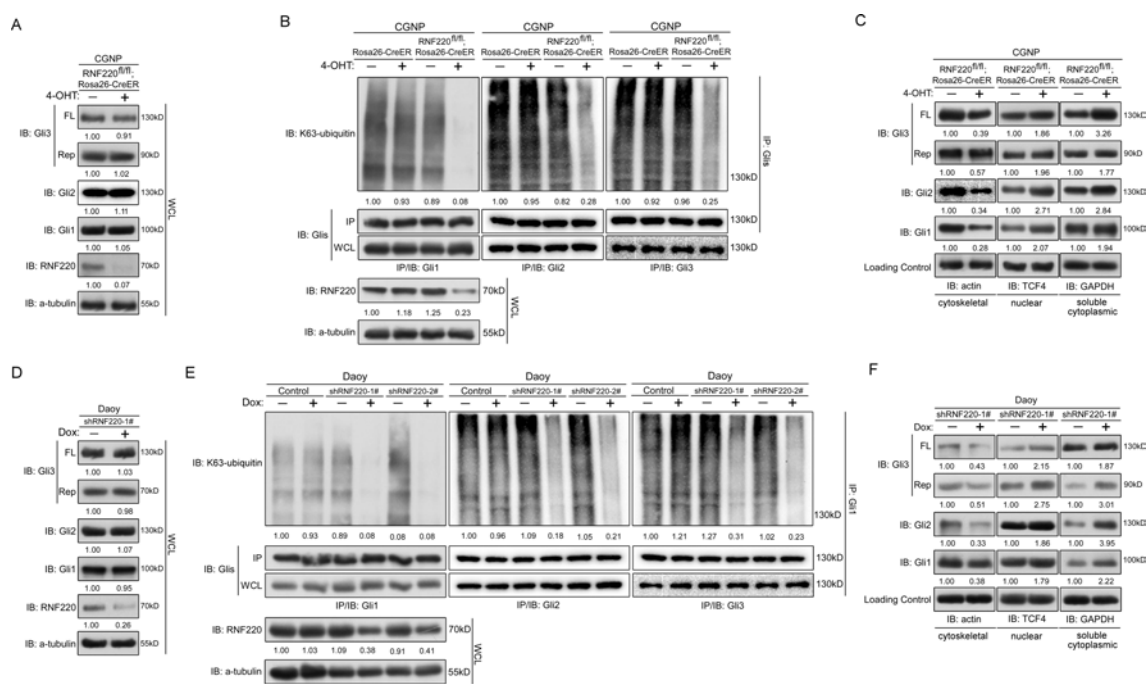


Figure S3. RNF220 targets Glis for K-63 linked polyubiquitination and promotes its nuclear exportation in both CGNPs and Daoy cells. (A) Western blot results showing the effect of RNF220 knockout on all the Glis protein level in CGNP cells. (B) The level of K-63 ubiquitinated Glis in the CGNP cells when RNF220 was induced knockout or not. (C) Western blot assays showing the subcellular distribution of endogenous Glis in control or RNF220 knockout CGNP cells. (D) Western blot results showing the effect of RNF220 knockdown on all the Glis protein level in Daoy cells. (E) The level of K-63 ubiquitinated Glis in the Daoy cells when RNF220 was induced knockdown or not. (F) Western blot assays showing the subcellular distribution of endogenous Glis in control or RNF220 knockdown Daoy cells. The protein level was quantified against α -tubulin followed by each control and the statistics were shown below each panel. IP, immunoprecipitation; WCL, whole cell lysate; IB, immunoblot.

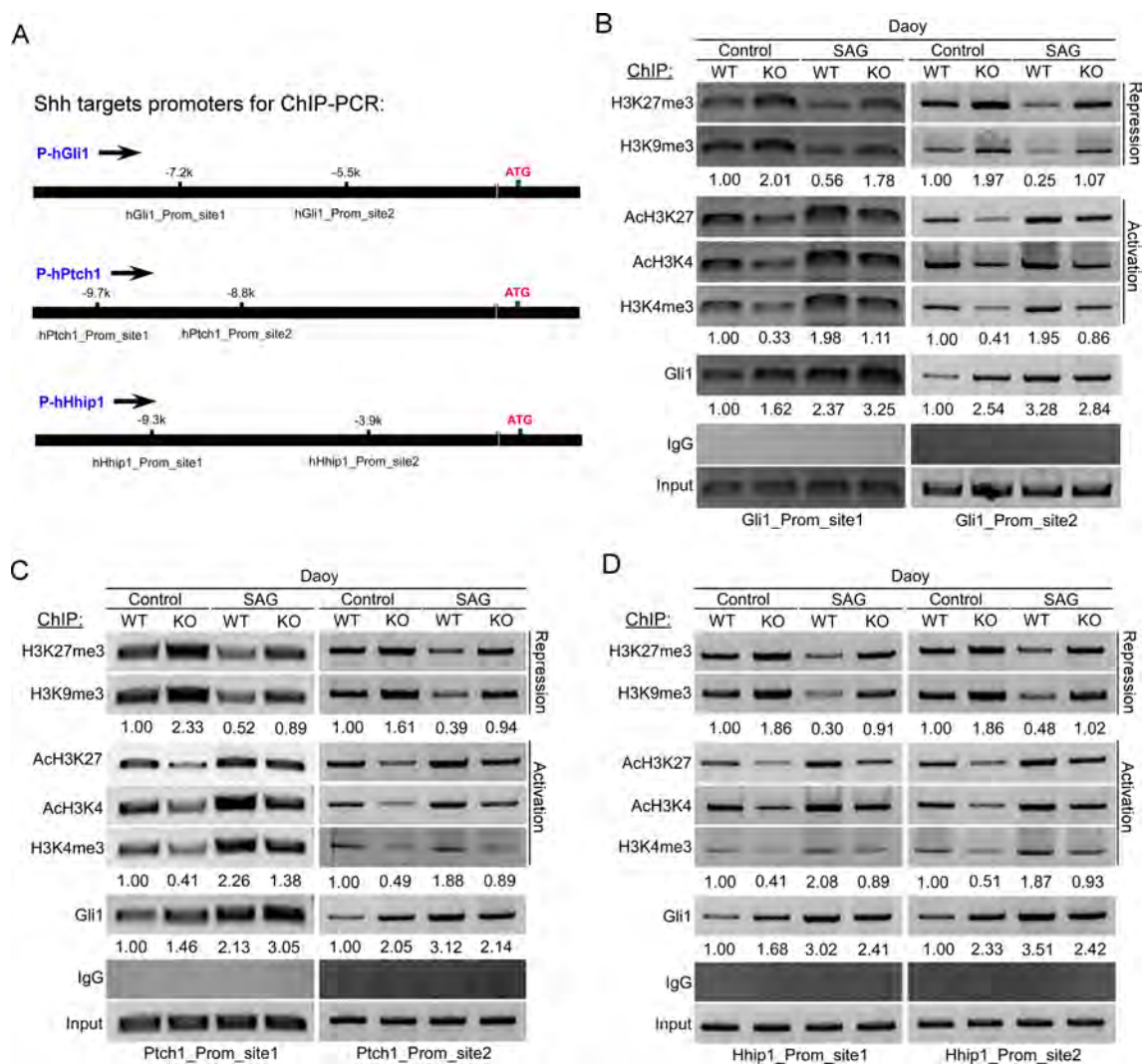


Figure S4. RNF220 knockdown alters epigenetic modification on

the promoter of Shh signaling targets in Daoy cells. (A) Schematic representation of the tested Gli binding sites in mouse Gli1, Ptch1 and Hhip1 promoters. The coordinates refer to the translational start codon. (B-D) Semi-quantification ChIP-PCR analysis of histone modification marks at the indicated Gli binding sites in Gli1 (B), Ptch1 (C) and Hhip1 (D) promoters in Daoy cells when endogenous RNF220 was knocked down. Dox was used to induce endogenous RNF220 knockdown in shRNF220 stably transfected Daoy cells. Note that for each repressive or activating group, the averaged relative levels of the different marks were shown.

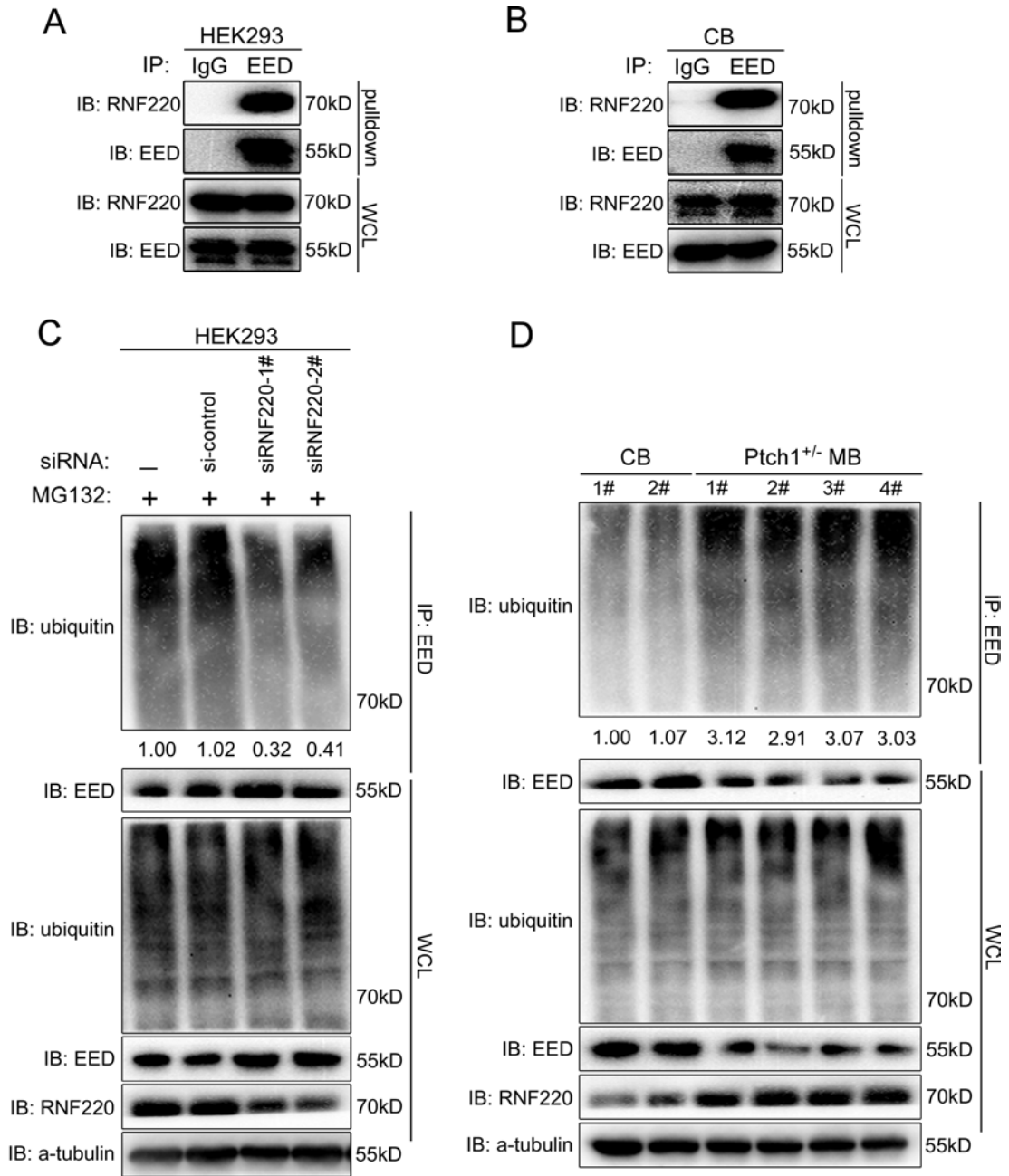


Figure S5. RNF220 interacts with EED and targets EED for

polyubiquitination and degradation. (A and B) Endogenous RNF220 was pulled down by EED in both HEK293 cells (A) and control cerebellum (B). (C) The polyubiquitination level of endogenous EED protein reduced when RNF220 was knocked down in HEK293 cells. (D) The ubiquitination level of endogenous EED protein in control cerebellum and *Ptch1*^{+/-} medulloblastoma tissues. The protein level was quantified against α -tubulin followed by each control and the statistics were shown below the indicated panels. WCL, whole cell lysate. IP, immunoprecipitation. IB, immunoblot.

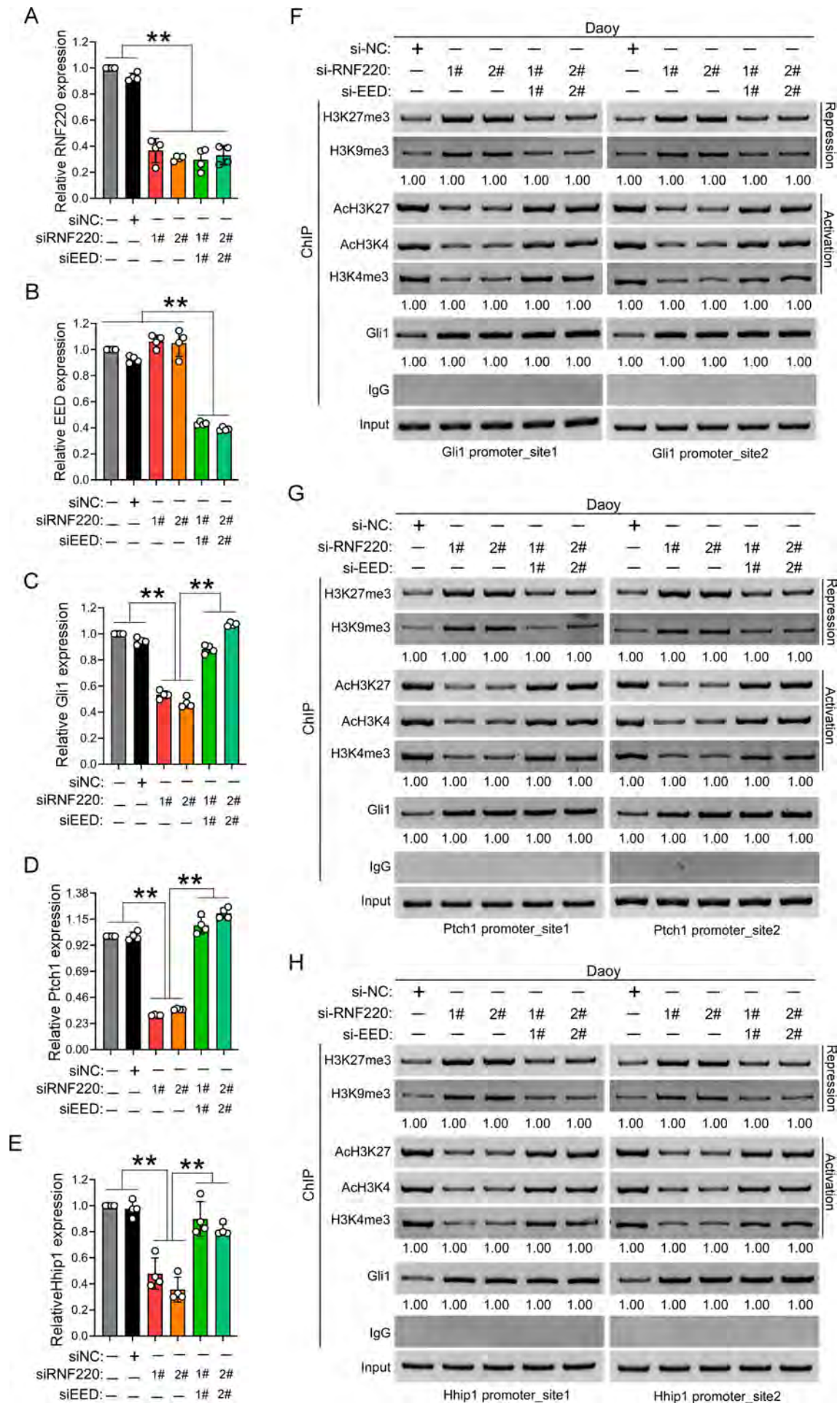


Figure S6. EED knockdown rescue RNF220 knockdown mediated

Shh signaling repression and epigenetic modification changes on the promoters of

Shh signaling targets in Daoy cells. (A-E) Realtime PCR assays showed the relative

expression level of RNF220 (A), EED (B), Gli1 (C), Ptch1 (D) and Hhip1 (E) when

the indicated siRNAs were transfected into the Daoy cells. (F-H) Semi-quantification

ChIP-PCR analysis of histone modification marks at the indicated Gli binding sites in

Gli1 (F), Ptch1 (G) and Hhip1 (H) promoters in Daoy cells. The indicated siRNAs

were used to knockdown the endogenous RNF220 or EED in Daoy cells. Cells were

harvested at 72 hours after siRNAs transfection and followed by nuclear purification,

chromosome fragments and immuniprecipitation with the indicated antibodies. Note

that for each repressive or activating group, the averaged relative levels of the

different marks were shown.

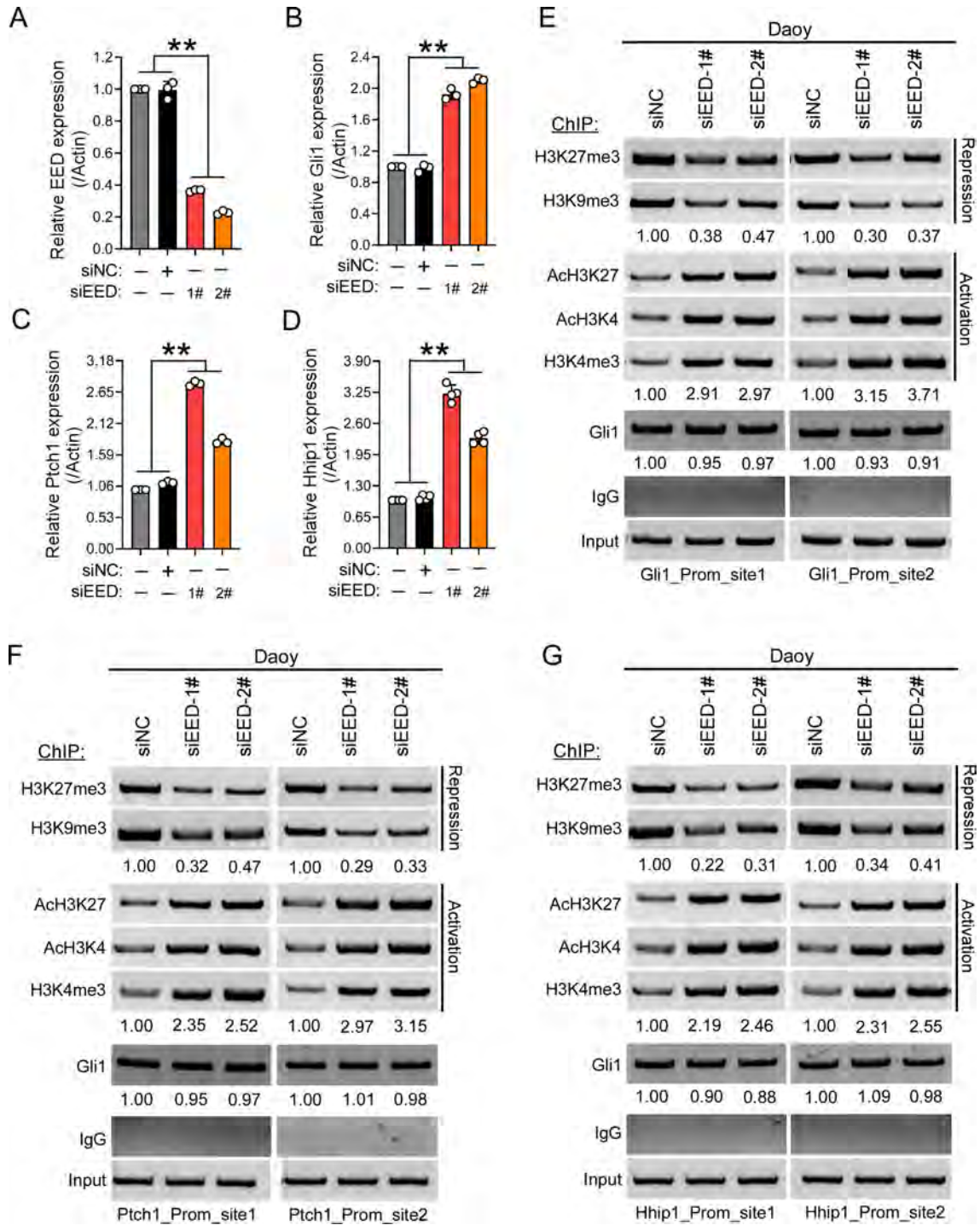


Figure S7. EED knockdown inhibits Shh signaling and changes the epigenetic modification on the promoters of Shh signaling targets in Daoy cells. (A-D) Realtime PCR assays showed the relative expression level of EED (A), Gli1 (B), Ptch1 (C) and Hhip1 (D) when the endogenous EED was knocked down in Daoy cells. (E-G) Semi-quantification ChIP-PCR analysis of histone modification marks at the indicated Gli binding sites in Gli1 (E), Ptch1 (F) and Hhip1 (G) promoters in Daoy cells when endogenous EED was knocked down. Note that for each repressive or activating group, the averaged relative levels of the different marks were shown.

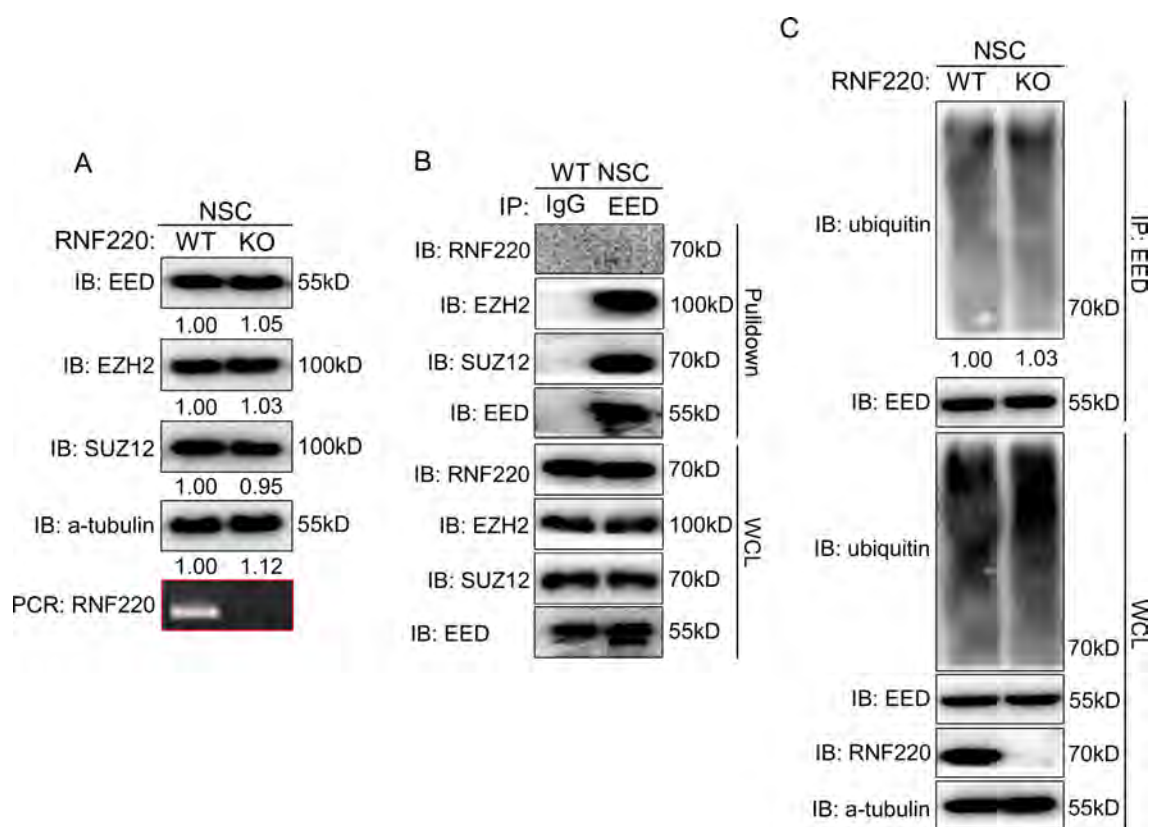


Figure S8. Effect of RNF220 knockout on EED protein levels and

epigenetic modification of Shh target genes in NSCs. (A) Western blotting of the PRC2 complex protein levels in control and RNF220 knockout NSC. (B) Co-IP assays shows the interaction between EED and the indicated proteins. In NSC, EED could pull down the other PRC2 complex member, such as EZH2 and SUZ12, but not RNF220. (C) The polyubiquitination level of endogenous EED is comparable between wildtype and RNF220 knockout NSC. The protein level was quantified against α -tubulin followed by each control and the statistics were shown below the indicated panel. IB, immunoblot; IP, immunoprecipitation; WCL, whole cell lysate.

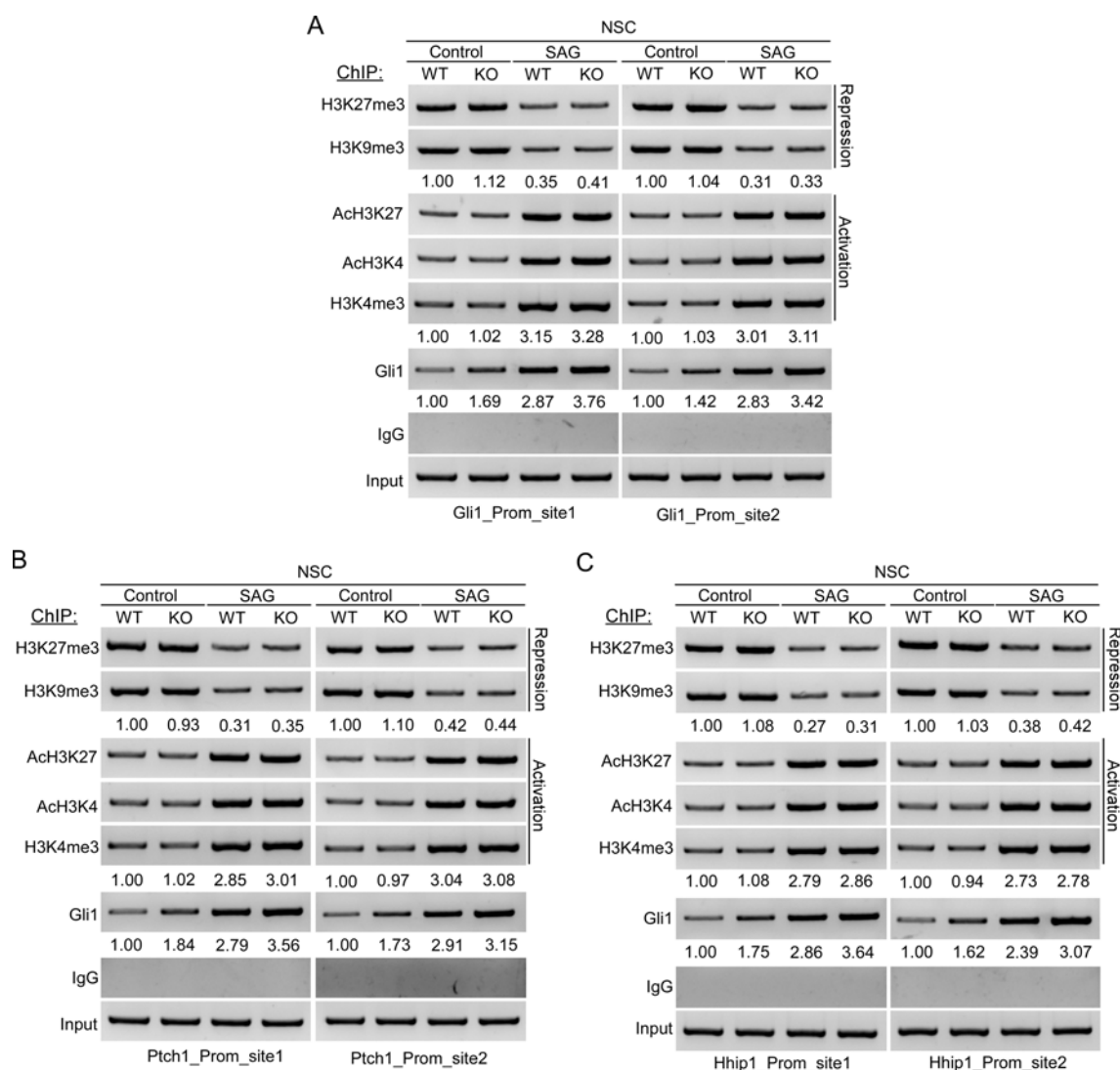


Figure S9. Effect of RNF220 knockout on epigenetic modification

marks at Gli binding sites in NSCs. Semi-quantification ChIP-PCR analysis of histone modification marks at the indicated Gli binding sites in the mouse Gli1 (A), Ptch1 (B) and Hhip1 (C) promoters in control or RNF220 knockout NSC. Note that for each repressive or activating group, the averaged relative levels of the different marks were shown.

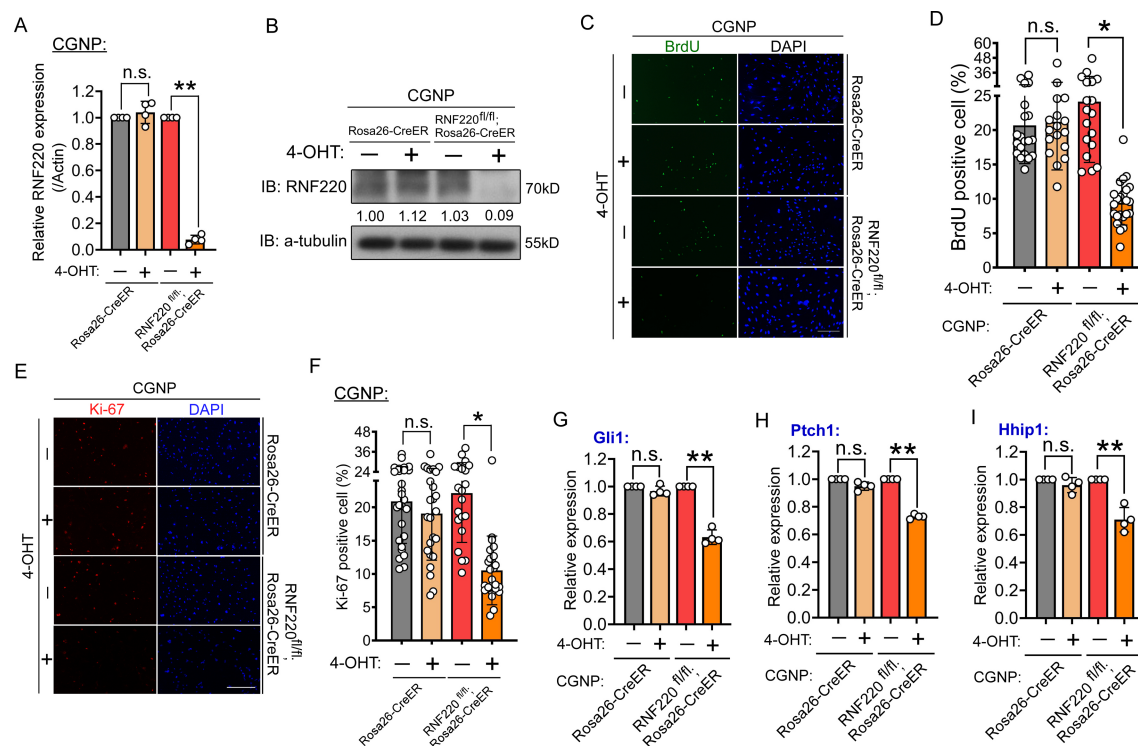


Figure S1. RNF220 knockout inhibits CGNP proliferation. (A and

B) Real-time PCR (A) and western blotting (B) showing the 4-OHT induced RNF220 knockout efficiency in CGNP cells. IB, immunoblot. (C-F) BrdU incorporation (C and D) and Ki-67 (E and F) staining assays to evaluate DNA synthesis and proliferation rates of CGNPs when RNF220 was knocked out by 4-OHT induction. Scale bar, 80 μ m. Quantification were shown in (D) and (E) respectively. (G-I) Realtime PCR assays show the relative expression level of Gli1(G), Ptch1 (H) and Hhip1 (I) in CGNP cells when RNF220 knock out was induced by 4-OHT incubation or not. Data are presented as the means \pm SD. n.s., no significant difference; * $p < 0.05$; ** $p < 0.01$.

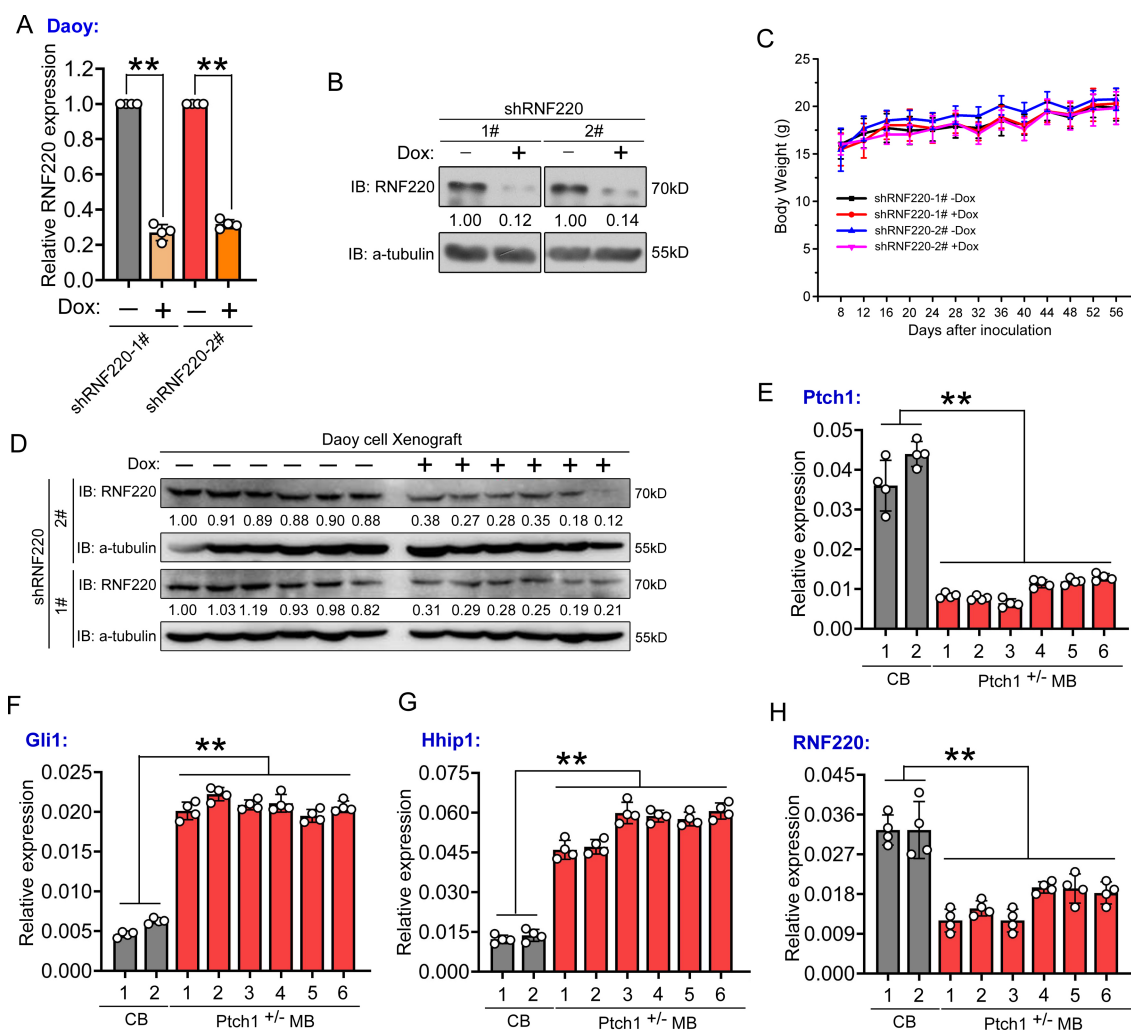


Figure S2. RNF220 knockdown efficiency and mRNA levels of Gli1,

Ptch1, Hhip1 and RNF220 in Ptch1^{+/-} MB tissues. (A and B) Real-time PCR (A) and

western blotting (B) showing the Dox-induced RNF220 knockdown efficiency in

shRNF220-1# or 2# stable Daoy cell lines. (C) Mice body weight was measured every

four days after shRNF220-1# or 2# clones were injected subcutaneously into BALB/c

nude mice and mice were fed with or without Dox. (D) RNF220 protein levels in

tumor tissues were detected by western blotting. The protein level was quantified

against α -tubulin followed by each control and the statistics were shown below each

panel. IB, immunoblot. (E–H) Real-time PCR of the relative expression of Ptch1 (E),

Gli1 (F), Hhip1 (G) and RNF220 (H) in control cerebellum and Ptch1^{+/-} MB tissues.

Data are presented as the means \pm SD. ** $p < 0.01$.

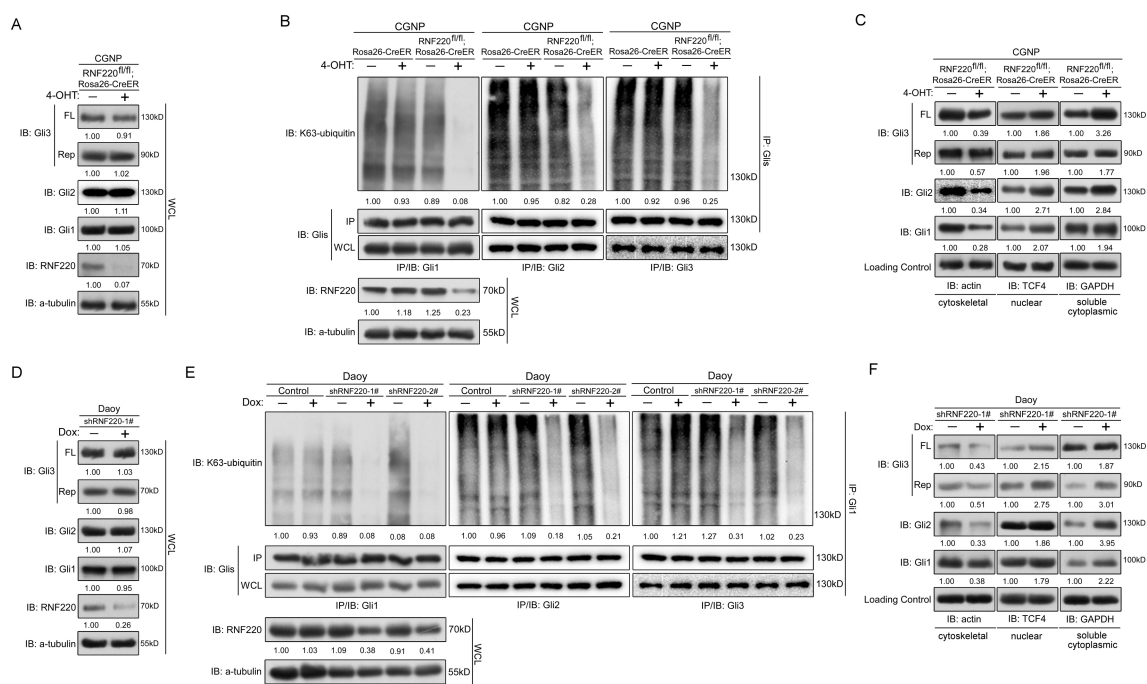


Figure S3. RNF220 targets Glis for K-63 linked polyubiquitination

and promotes its nuclear export in both CGNPs and Daoy cells. (A) Western blot results showing the effect of RNF220 knockout on all the Glis protein level in CGNP cells. (B) The level of K-63 ubiquitinated Glis in the CGNP cells when RNF220 was induced knockout or not. (C) Western blot assays showing the subcellular distribution of endogenous Glis in control or RNF220 knockout CGNP cells. (D) Western blot results showing the effect of RNF220 knockdown on all the Glis protein level in Daoy cells. (E) The level of K-63 ubiquitinated Glis in the Daoy cells when RNF220 was induced knockdown or not. (F) Western blot assays showing the subcellular distribution of endogenous Glis in control or RNF220 knockdown Daoy cells. The protein level was quantified against α -tubulin followed by each control and the statistics were shown below each panel. IP, immunoprecipitation; WCL, whole cell lysate; IB, immunoblot.

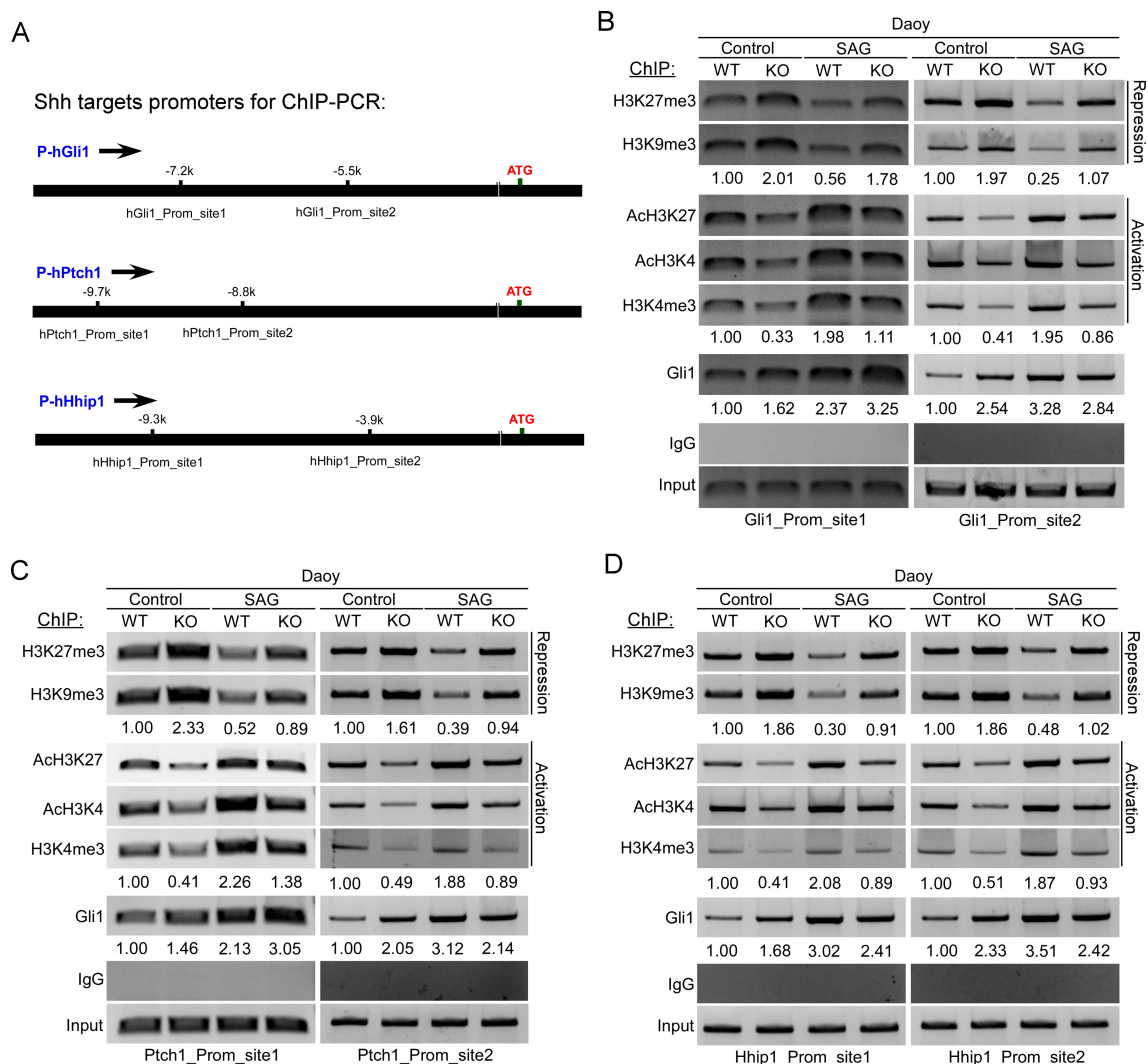


Figure S4. RNF220 knockdown alters epigenetic modification on

the promoter of Shh signaling targets in Daoy cells. (A) Schematic representation of the tested Gli binding sites in mouse Gli1, Ptch1 and Hhip1 promoters. The coordinates refer to the translational start codon. (B-D) Semi-quantification ChIP-PCR analysis of histone modification marks at the indicated Gli binding sites in Gli1 (B), Ptch1 (C) and Hhip1 (D) promoters in Daoy cells when endogenous RNF220 was knocked down. Dox was used to induce endogenous RNF220 knockdown in shRNF220 stably transfected Daoy cells. Note that for each repressive or activating group, the averaged relative levels of the different marks were shown.

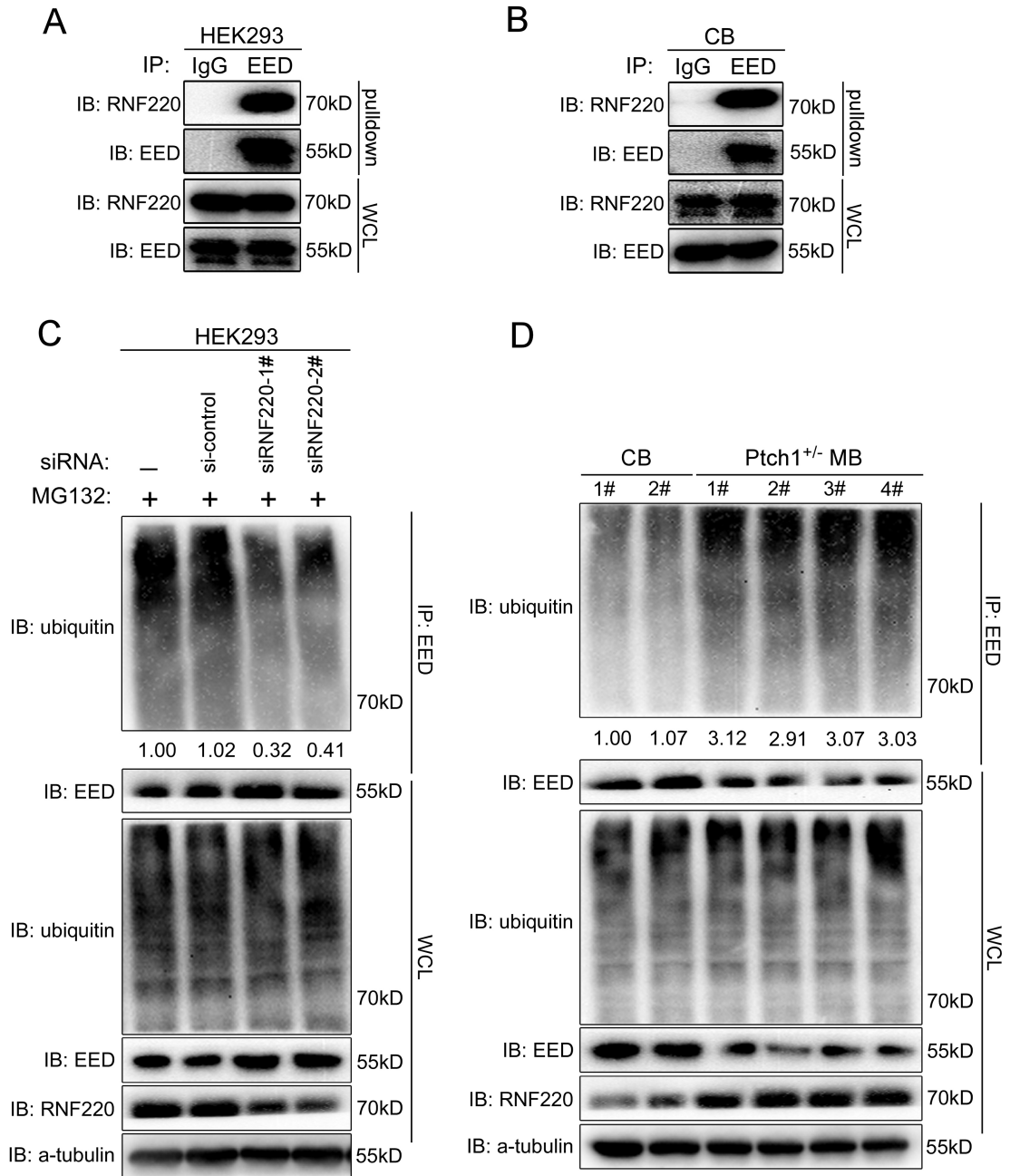


Figure S5. RNF220 interacts with EED and targets EED for

polyubiquitination and degradation. (A and B) Endogenous RNF220 was pulled down by EED in both HEK293 cells (A) and control cerebellum (B). (C) The polyubiquitination level of endogenous EED protein reduced when RNF220 was knocked down in HEK293 cells. (D) The ubiquitination level of endogenous EED protein in control cerebellum and *Ptch1*^{+/-} medulloblastoma tissues. The protein level was quantified against α -tubulin followed by each control and the statistics were shown below the indicated panels. WCL, whole cell lysate. IP, immunoprecipitation. IB, immunoblot.

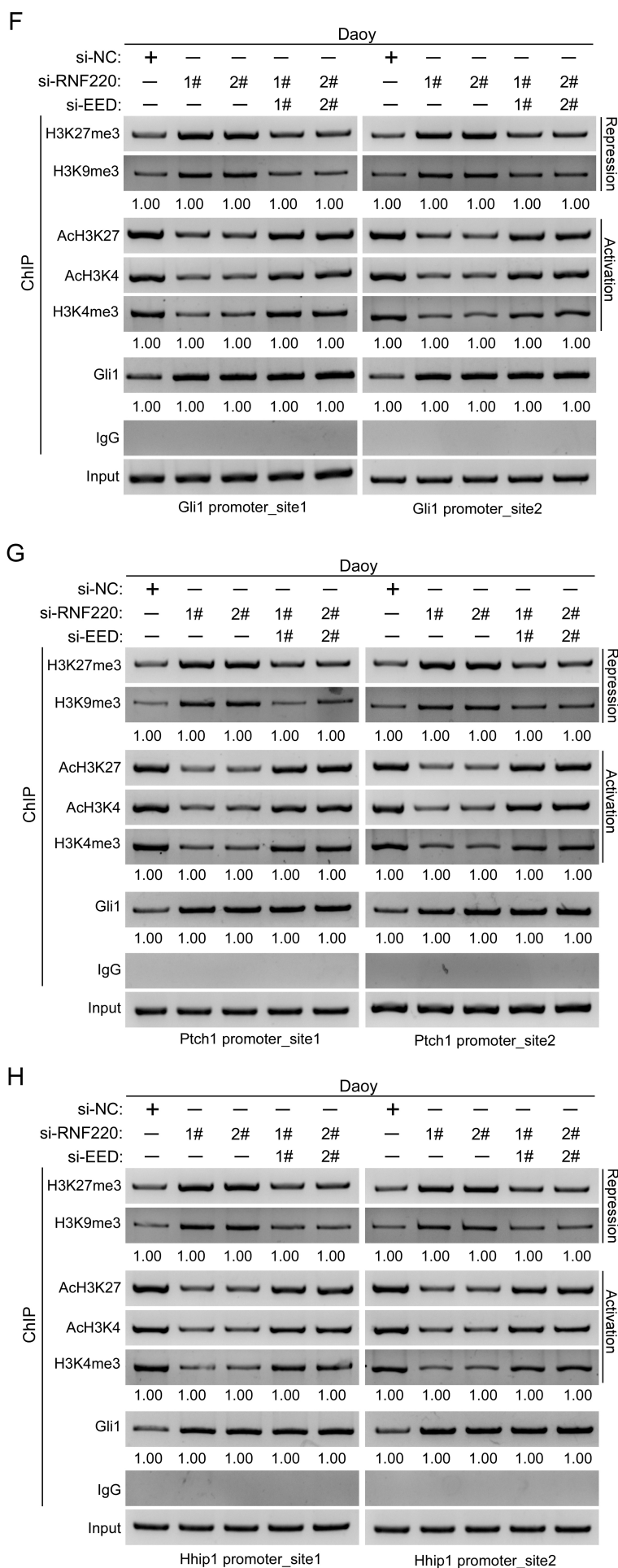
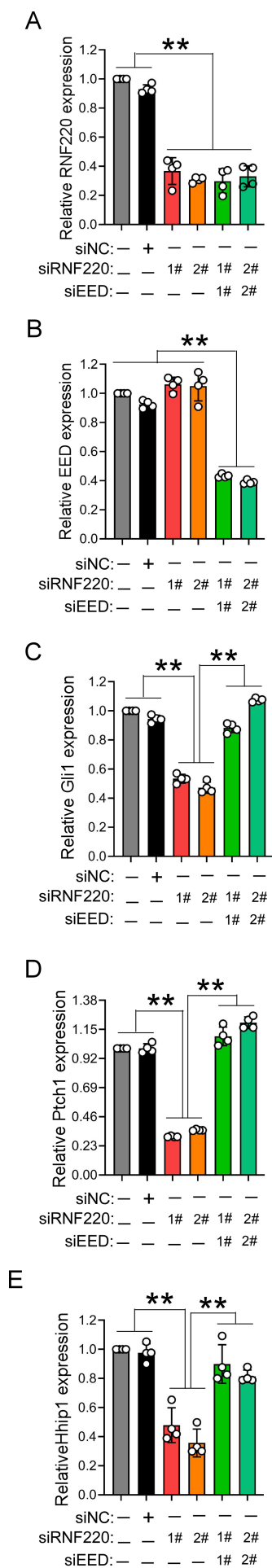


Figure S6. EED knockdown rescue RNF220 knockdown mediated

Shh signaling repression and epigenetic modification changes on the promoters of

Shh signaling targets in Daoy cells. (A-E) Realtime PCR assays showed the relative

expression level of RNF220 (A), EED (B), Gli1 (C), Ptch1 (D) and Hhip1 (E) when

the indicated siRNAs were transfected into the Daoy cells. (F-H) Semi-quantification

ChIP-PCR analysis of histone modification marks at the indicated Gli binding sites in

Gli1 (F), Ptch1 (G) and Hhip1 (H) promoters in Daoy cells. The indicated siRNAs

were used to knockdown the endogenous RNF220 or EED in Daoy cells. Cells were

harvested at 72 hours after siRNAs transfection and followed by nuclear purification,

chromosome fragments and immuniprecipitation with the indicated antibodies. Note

that for each repressive or activating group, the averaged relative levels of the

different marks were shown.

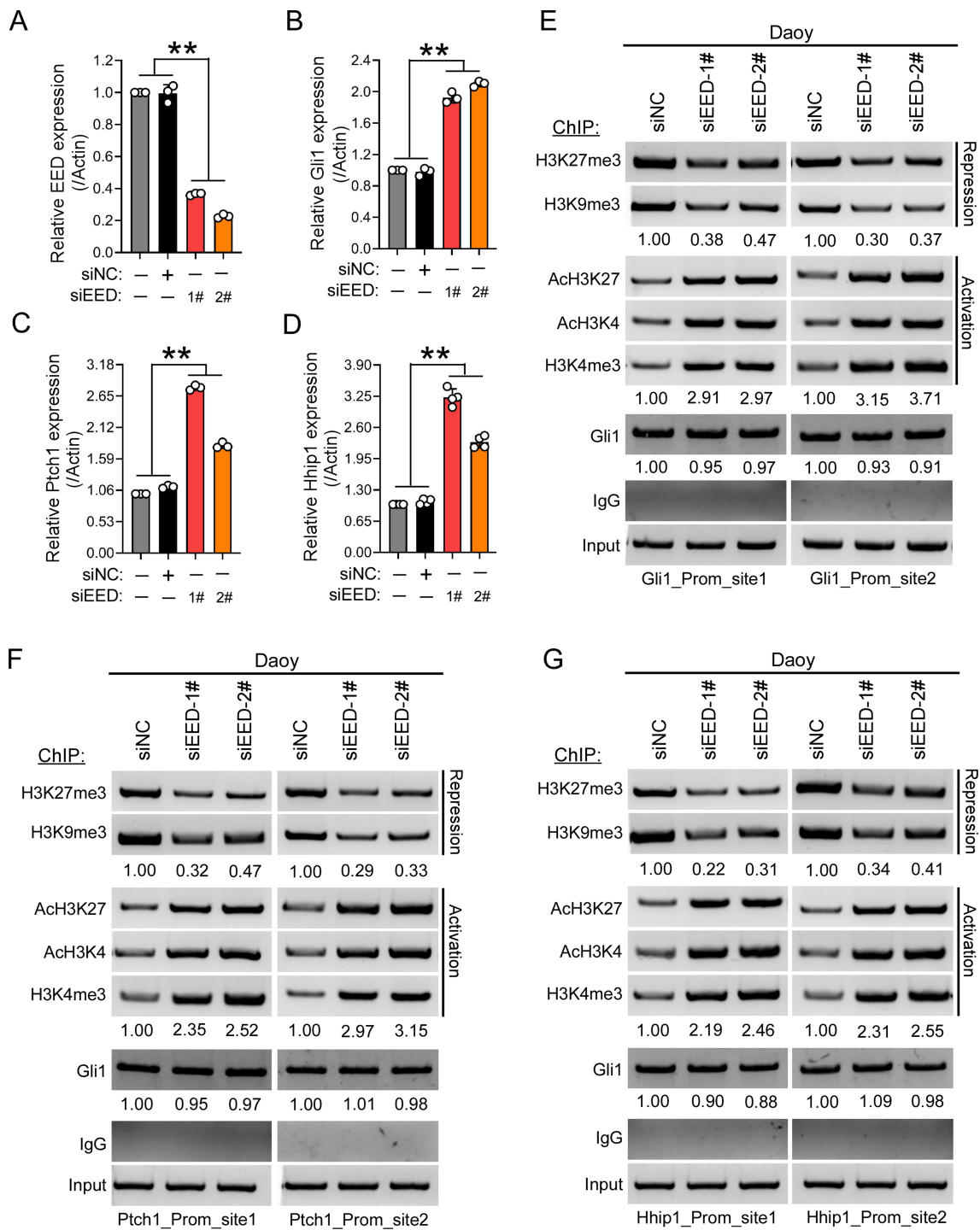


Figure S7. EED knockdown inhibits Shh signaling and changes the epigenetic modification on the promoters of Shh signaling targets in Daoy cells. (A-D) Realtime PCR assays showed the relative expression level of EED (A), Gli1 (B), Ptch1 (C) and Hhip1 (D) when the endogenous EED was knocked down in Daoy cells. (E-G) Semi-quantification ChIP-PCR analysis of histone modification marks at the indicated Gli binding sites in Gli1 (E), Ptch1 (F) and Hhip1 (G) promoters in Daoy cells when endogenous EED was knocked down. Note that for each repressive or activating group, the averaged relative levels of the different marks were shown.

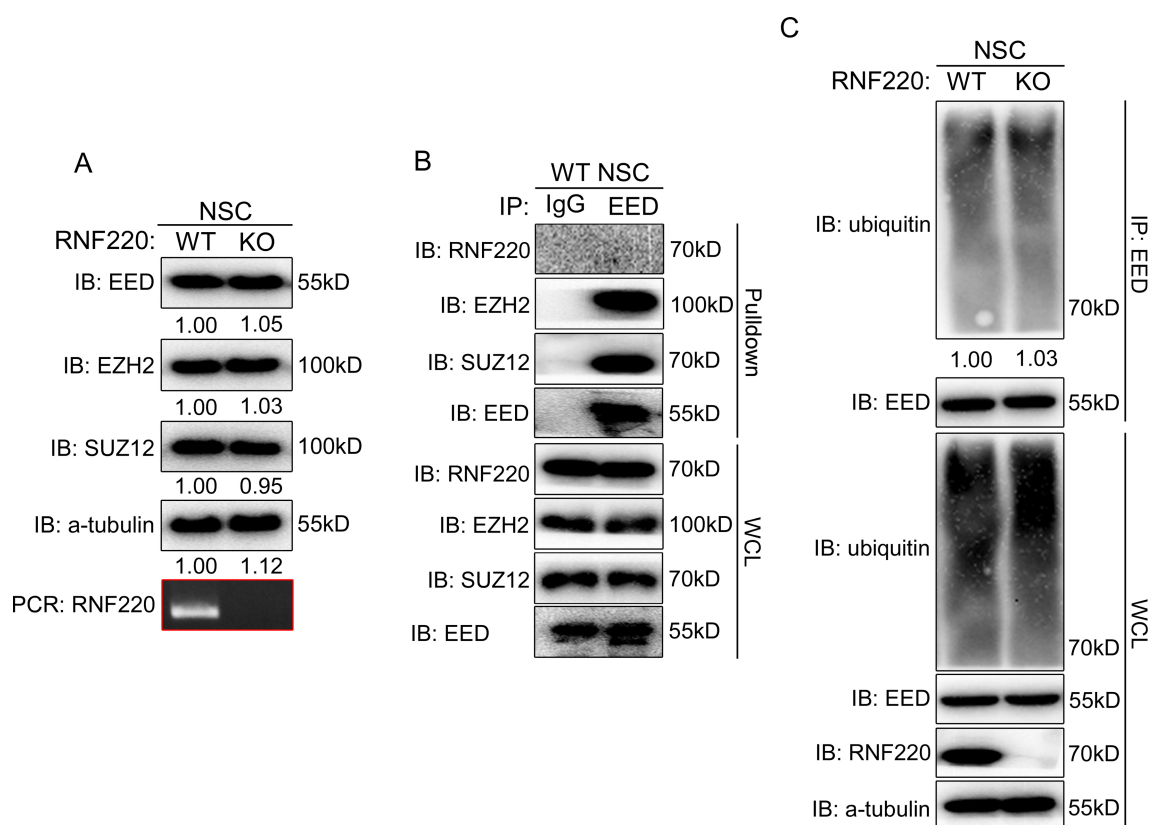


Figure S8. Effect of RNF220 knockout on EED protein levels and

epigenetic modification of Shh target genes in NSCs. (A) Western blotting of the PRC2 complex protein levels in control and RNF220 knockout NSC. (B) Co-IP assays shows the interaction between EED and the indicated proteins. In NSC, EED could pull down the other PRC2 complex member, such as EZH2 and SUZ12, but not RNF220. (C) The polyubiquitination level of endogenous EED is comparable between wildtype and RNF220 knockout NSC. The protein level was quantified against α -tubulin followed by each control and the statistics were shown below the indicated panel. IB, immunoblot; IP, immunoprecipitation; WCL, whole cell lysate.

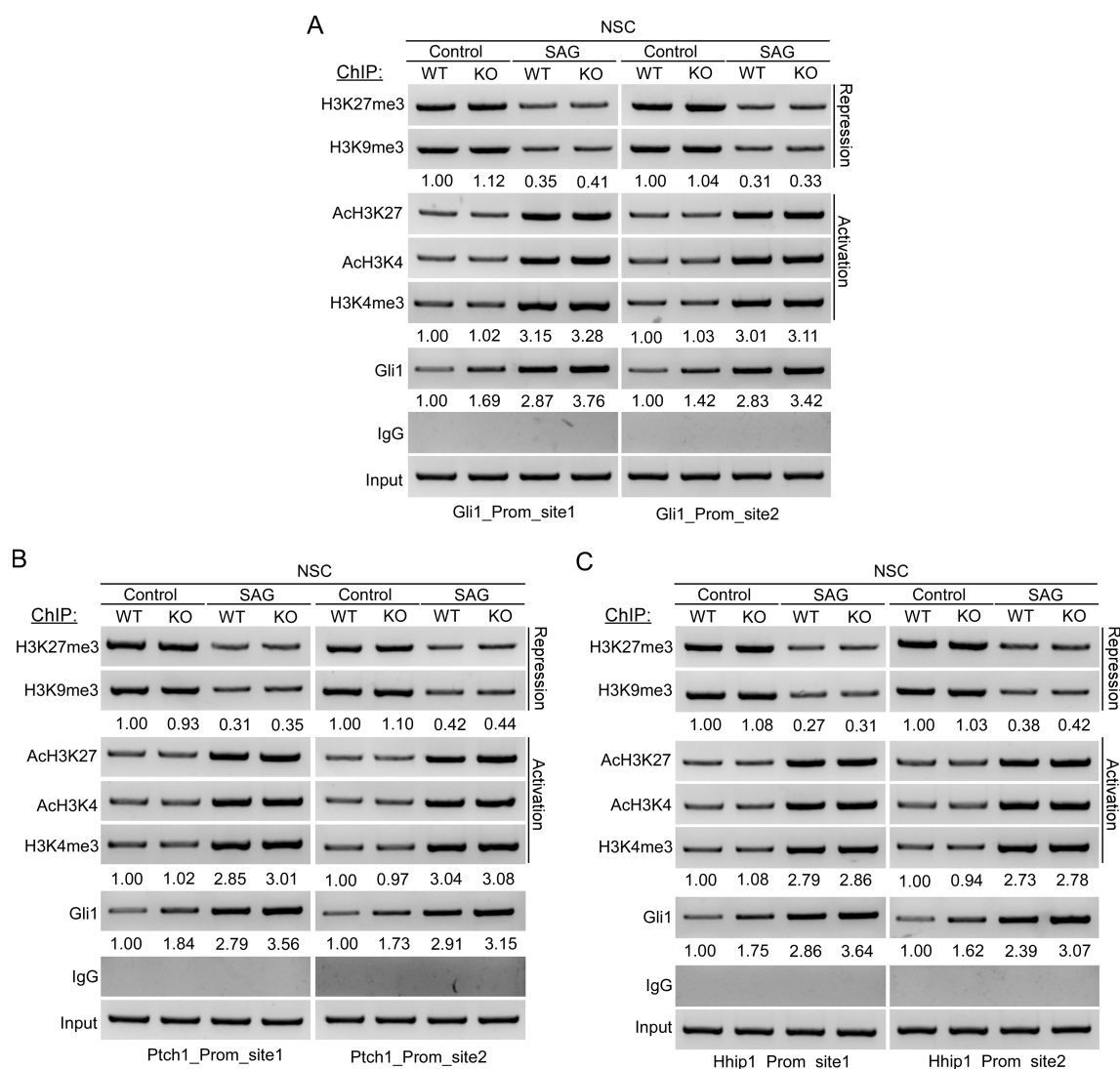


Figure S9. Effect of RNF220 knockout on epigenetic modification

marks at Gli binding sites in NSCs. Semi-quantification ChIP-PCR analysis of histone modification marks at the indicated Gli binding sites in the mouse Gli1 (A), Ptch1 (B) and Hhip1 (C) promoters in control or RNF220 knockout NSC. Note that for each repressive or activating group, the averaged relative levels of the different marks were shown.